

CBPF

MASTER THESIS

Entanglement in Coarse-grained Systems

Author:
Pedro CORREIA

Supervisor:
Dr. Fernando DE MELO

*A thesis submitted in fulfillment of the requirements
for the degree of Master in Physics*

in the

Quantum Information Group - CBPF
Theoretical Physics department

August 28, 2017

CBPF

Abstract

Quantum Information Group - CBPF
Theoretical Physics department

Master in Physics

Entanglement in Coarse-grained Systems

by Pedro CORREIA

In the present work we investigate an effective description of entanglement in spin-chains when we do not have access to all degrees of freedom of the system. More specifically, inspired by an experimental situation, we developed a coarse graining approach that describes the detection of a spin-chain taking into account a "blurred" detector that does not have sufficient resolution to resolve single sites in the lattice. We constructed a coarse graining map that takes the information from neighboring sites as a single site. Such idea allows us to study the entanglement behavior taking into account different ranges of resolution of the spin chain and entanglement detectability. In the second part we derive an equation for entanglement in 2xD systems, when the D-dimensional part undergoes a coarse graining channel. Such situation can illustrate the measurement process, when a detector (macroscopic object, D-dimensional system), in which we handle only few effective degrees of freedom, interacts with a quantum system (2-dimensional system). Then we see how the entanglement behaves as the detector increases (D increases). This approach can shed light on the quantum-to-classical transition problem.

Contents

Abstract	iii
1 Introduction	1
2 Features of Quantum Mechanics and Entanglement	3
2.1 Physical Systems in Quantum Mechanics	3
2.1.1 Pure States	3
2.1.2 Mixed States	4
2.1.3 Composite Quantum systems	5
2.1.4 Reduced Density operator	5
2.2 Quantum Operations	6
2.2.1 Completely positive maps	6
Linear maps	6
Completely positive maps	6
2.2.2 Defining Quantum Operations	7
2.2.3 Coarse Graining Channel	8
A Blurred Detector	9
2.3 Entangled States	10
2.3.1 Entangled Pure States	10
2.3.2 Entangled Mixed States	10
2.4 Separability Criteria	11
2.4.1 Pure States	11
Schmidt decomposition	11
2.4.2 Mixed States	12
Positive Maps	12
Peres-Horodecki criterion	13
2.5 Entanglement Monotones and Measures	14
2.5.1 Local Operations and Classical Communication (LOCC)	14
)	14
Invariance of Entanglement Under Local Unitaries	15
2.5.2 Entanglement Measures	15
Entanglement Entropy	16
Concurrence	17
Negativity	18
3 Spin-Entanglement in a Coarse-Grained Optical Lattice	19
3.1 Spin-entanglement Dynamics in a Bose-Hubbard Chain	20
3.1.1 Storing Atoms in Optical Lattice	20
Light-atom interaction	20
Bose-Hubbard Systems	22
Superfluid to Mott insulator Phase Transition	23
3.1.2 Local Detection in an atomic Mott insulator	23
Fluorescence Imaging	23
Single-Spin Addressing	25

3.1.3	Entanglement during spin-impurity dynamics	26
	Concurrence between two sites	26
3.1.4	Measuring a Lower Bound for Concurrence	27
	Experimental Procedure	27
	Lower Bound for Concurrence	29
3.2	Coarse-grained Entanglement in a Spin Chain	31
3.2.1	Coarse-Grained Entanglement Dynamics	32
	Concurrence	33
	Negativity	35
4	Equation for Entanglement in Coarse-grained Systems	39
4.1	Evolution Equation for Quantum Entanglement	39
4.1.1	Entanglement Under Filtering Operations	40
4.1.2	Evolution Equation for concurrence of $2 \times D$ systems	41
4.1.3	A Statistical Approach of Entanglement Evolution in $2 \times D$ Systems	44
4.2	Entanglement in $2 \times D$ Coarse Grained Systems	46
5	Conclusion and Perspectives	51
6	Appendix	53
6.1	Probability Theory	53
6.1.1	Covariance and Variance	53
6.1.2	Covariance Inequality	53
	Bibliography	55

Chapter 1

Introduction

Quantum theory describes the microscopic world: such as atoms, ions, electrons, photons, etc. Quantum systems made of a single particle display properties that are unknown to classical ones, such as interference, tunnelling or superposition of states. Furthermore, composite quantum systems can exist in a superposition of many particle states. This leads to an intrinsic quantum correlation of the individual constituents in which measurements on each part of the system can exhibit strong correlations that cannot be achieved classically. This kind of quantum correlation is called entanglement [24].

In realistic situations the role of the entanglement is crucial to the description of many body quantum systems. The larger the quantum system, the more difficult it is to isolate it from the environment, resulting in a pronounced decoherence process. That is, in the interaction system-environment, the system loses information to the environment faster the larger the system. In this way the quantitative description of the entanglement dynamics offers a good indicator of the decoherence process. Furthermore, the entanglement is one of the resources for quantum information [5] so that its microscopic control is necessary in many applications: from quantum computation [26] to quantum communication protocols [31, 6].

Experimentally, the measurement of entanglement is a challenge. Realizations with full quantum state tomography [36] are feasible only in small systems [37, 27], since it requires remarkable control and resources. In larger many-body systems its presence can be inferred by macroscopic observables [3, 14, 33], but usually it is a difficult task to give a quantitative description of the entanglement.

Currently spin systems realized with ultracold atoms in optical lattices are a prominent well-controlled quantum system that offer the possibility of exploring local detection of entanglement [18] without performing full state tomography. In this framework a single site detection of spin-entanglement in a Bose-Hubbard chain can be achieved by fluorescence imaging [39]. However, in special for this single site resolution, the experimental realizations spend high experimental resource. The local detection by fluorescence [39] requires highly accurate equipments, like high-resolution microscopy, that can become an obstacle. In order to make the experimental procedure simpler and more feasible, a question arises: Given an entangled spin-system, is it possible to have a satisfactory description of the spin-entanglement if we aren't able to fully resolve the system?

In the first part of this work it will be shown a suitable proposal to answer the above question. Inspired by the experimental situation in [18], we will develop a proposal that describes the detection of the spin chain taking

into account a "blurred" detector that does not have sufficient resolution to resolve single sites in the lattice. Such idea allows us to study the entanglement behavior taking into account different ranges of resolution of the spin chain. In the quantum information scheme the "blurred" detector will be mapped by a quantum operation that takes quantum states to a lower dimensional Hilbert space. As we will see, this kind of operation is called a coarse-graining operation, and we relate to the "blurred" chain, as a coarse-grained chain.

In the second part, inspired by works [43, 29, 44, 42], we will start deriving an equation for entanglement dynamics in $2 \times D$ systems where the D -dimensional part undergoes a dynamical process. Such equation takes minimal information about the initial state and the quantum channel related to the dynamical process. From this result, we consider as the dynamical channel the developed coarse-graining process. Such situation illustrates the measurement process, where a detector (D -dimensional system) interacts with a qubit (2-dimensional system) to be measured, and they become a $2 \times D$ entangled system. So the coarse graining operation over the d -dimensional part illustrates the fact that the experimentalist can not control all of D degrees of freedom of the detector system. Instead, they handle only few effective degrees d (usually $d \ll D$). So, in this approach we expect to lose quantum information the larger is the detector size.

Chapter 2

Features of Quantum Mechanics and Entanglement

The purpose of this chapter is to provide a short review of the main concepts and tools in quantum mechanics that will be useful for this work.

In the first section (2.1), we will show how physical systems are described in quantum mechanics. And then, differentiate quantum states into two categories: pure and mixed. In doing this, it will be presented a more general formalism that describes quantum states as matrices, instead of vector states. As we shall see, this representation, called density operator (or density matrix), is essential to describe mixed states, besides that some useful operations are only feasible in this formalism.

In the second section (2.2) we will show how can we describe a general transformation in quantum systems. In this way it will be presented a general tool for describing transformations over quantum system, called quantum operation formalism [31].

Finally, in the third section (2.3) an important property of composite quantum system will be shown: the entangled states. As well in classical systems, quantum systems composed of, at least, two subsystems can display correlations between their parts. However, if a quantum system satisfies certain conditions, a strictly quantum correlations appear. The systems that display this "special" quantum correlations between their parts are called entangled states.

2.1 Physical Systems in Quantum Mechanics

The way a physical system is described in a quantum approach is the target of the first postulate of quantum mechanics. According to the first postulate of quantum mechanic, to every physical system, a Hilbert \mathcal{H} (complex vector space with inner product) is associated. So that the quantum state of an isolated system a normalized vector $|\Psi\rangle \in \mathcal{H}$ is assigned. With the vector state $|\Psi\rangle$, we can know everything possible about the system.

2.1.1 Pure States

If the system can be described by a single space vector $|\psi\rangle$ we say that the system is in a pure state. An usual example of pure state in quantum computation is a pure qubit state, that is, the unit of quantum information (the quantum analogue of the classical bit of information). A qubit is characterized by a two-level quantum system, $|\psi\rangle \in \mathbb{C}^2$. The vector $|\psi\rangle$ can be expressed as a linear combination of orthonormal basis vectors $|0\rangle$ and $|1\rangle$

with $\alpha, \beta \in \mathbb{C}$:

$$|\psi\rangle = \alpha|0\rangle + \beta|1\rangle. \quad (2.1)$$

The coefficients α and β are known as the probabilities amplitudes related to $|0\rangle$ and $|1\rangle$ respectively.

Since we interpret α and β as probabilities amplitudes, thus $|\psi\rangle$ must be a normalized state vector:

$$\langle\psi|\psi\rangle = 1, \quad (2.2)$$

thus

$$|\alpha|^2 + |\beta|^2 = 1. \quad (2.3)$$

That is, $|\alpha|^2$ and $|\beta|^2$ are the probabilities of outcome $|0\rangle$ or $|1\rangle$ respectively and the equation above represents the total probability of all possible outcomes must be 1.

As known examples of two-level quantum systems, we have the polarization of a single photon, or the spin of a 1/2-spin particle.

2.1.2 Mixed States

Now, if the quantum system is an ensemble of pure states $\{p_i, |\psi_i\rangle\}$ (where p_i is the probability related to state $|\psi_i\rangle$), we say that the system is in a mixed state. Considering a measurement, the expectation value of some observable A on a mixed state is given by

$$\begin{aligned} \langle A \rangle &= \sum_i p_i \langle \psi_i | A | \psi_i \rangle \\ &= \text{tr} \left[\left(\sum_i p_i |\psi_i\rangle\langle\psi_i| \right) A \right]. \end{aligned} \quad (2.4)$$

Notice that, the term in parentheses contains only properties of the ensemble, independently of the observable in question. So it is convenient to define the density operator ψ as follows

$$\psi \equiv \sum_i p_i |\psi_i\rangle\langle\psi_i|, \quad (2.5)$$

which satisfy the trace condition

$$\text{tr}(\psi) = 1 \quad (2.6)$$

and the positivity condition

$$\langle\phi|\psi|\phi\rangle \geq 0, \quad (2.7)$$

with $|\phi\rangle$ is an arbitrary vector in \mathcal{H} . Usually the positivity condition is written simply as $\psi \geq 0$.

Pure states can also be represented by a density operator ψ , since the density operator formalism contains the state vector formalism. A pure state $|\psi\rangle$ is an ensemble specified by $p_i = 1$ for a single $|\psi_i\rangle = |\psi\rangle$ and $p_i = 0$ for all others $|\psi_i\rangle$, then $\psi = |\psi\rangle\langle\psi|$. A pure qubit represented by a density

operator becomes, by (2.1):

$$\psi = (\alpha|0\rangle + \beta|1\rangle)(\alpha\langle 0| + \beta\langle 1|) = \begin{pmatrix} |\alpha|^2 & \alpha\beta^* \\ \alpha^*\beta & |\beta|^2 \end{pmatrix}. \quad (2.8)$$

A question arises: given a density operator ψ , how can we determine if the state is pure or mixed? There is a simple test, from (2.4)

$$\psi^2 = \left(\sum_i p_i |\psi_i\rangle\langle\psi_i| \right) \left(\sum_j p_j |\psi_j\rangle\langle\psi_j| \right) = \sum_{ij} p_i p_j |\psi_i\rangle\langle\psi_i|\psi_j\rangle\langle\psi_j|. \quad (2.9)$$

If ψ is given in its spectral decomposition, we identify in (2.8) the kronecker delta $\langle\psi_i|\psi_j\rangle = \delta_{ij}$, so

$$\psi^2 = \sum_i p_i^2 |\psi_i\rangle\langle\psi_i|. \quad (2.10)$$

Now we will inspect the trace of ψ^2

$$\text{tr}\psi^2 = \sum_i p_i^2. \quad (2.11)$$

For pure states $\text{tr}\psi^2 = 1$, since there is only one nonzero p_i with value $p = 1$. However for mixed states there is more than one $p_i \neq 0$ with $0 < p_i < 1$, so $p_i^2 < p_i$ and leads to $\text{tr}\psi^2 < 1$. Summing up

- $\text{tr}\psi^2 = 1$ if only if ψ is a pure state
- $\text{tr}\psi^2 < 1$ if only if ψ is a mixed state

2.1.3 Composite Quantum systems

A composite system of N subsystems, also referred to a multipartite system, can be associated to a Hilbert space \mathcal{H} given by the tensor product of the spaces corresponding to each subsystems:

$$\mathcal{H} = \mathcal{H}_1 \otimes \cdots \otimes \mathcal{H}_N. \quad (2.12)$$

This scenario can be illustrated, for example, by a system of N spins located on lattice sites, where each spin corresponds to a subsystem that composes the lattice system.

In the following sections we shall focus in bipartite systems (composite systems composed only of two subsystems), formally represented by

$$\mathcal{H} = \mathcal{H}_A \otimes \mathcal{H}_B,$$

where $\mathcal{H}_A \equiv \mathcal{H}_1$ and $\mathcal{H}_B \equiv \mathcal{H}_2$. This simplification doesn't prevent that we can generalize the following results to arbitrary multipartite system.

2.1.4 Reduced Density operator

The density operator formalism provides a way to describe subsystems from a large system. This is possible by using a basic tool called partial trace, which map the density operator of a composite system into a reduced density operator of the desired subsystem.

Give a bipartite state $\psi \in \mathcal{H}_A \otimes \mathcal{H}_B$, its partial trace over the subsystem B is defined as

$$\text{tr}_B(|a_1\rangle\langle a_2| \otimes |b_1\rangle\langle b_2|) \equiv |a_1\rangle\langle a_2| \text{tr}(|b_1\rangle\langle b_2|), \quad (2.13)$$

where $\{|a\rangle_1, |a\rangle_2\} \in \mathcal{H}_A$ and $\{|b\rangle_1, |b\rangle_2\} \in \mathcal{H}_B$. Reciprocally, the partial trace over A is defined. Then the reduced density operator for system A is defined by

$$\psi_A \equiv \text{tr}_B \psi_{AB}. \quad (2.14)$$

Analogously $\psi_B = \text{tr}_A \psi_{AB}$.

The reduced density operator provides a way to deal with systems closer to real systems. Quantum systems are hardly completely isolated from the environment. The reduced density operator allows us to describe only the desired quantum system tracing out the environment from the total system.

2.2 Quantum Operations

In quantum mechanics, the quantum operation formalism describes the set of transformations that a quantum system can suffer. Roughly speaking, quantum operations are linear maps that must satisfy certain criteria to get physical sense. In this section we will see what are the properties that characterizes quantum operations and then some examples of this operations.

2.2.1 Completely positive maps

Linear maps

Basically, a linear map between two vector spaces \mathcal{V} and \mathcal{W} , with dimensions n and m respectively, is a map $\Lambda : \mathcal{V} \rightarrow \mathcal{W}$ that preserves the operations of addition and scalar multiplication:

- $\Lambda(A + B) = \Lambda(A) + \Lambda(B)$ for any matrices A and B in \mathcal{V}
- $\Lambda(\alpha A) = \alpha \Lambda(A)$ for any scalar α

If we look from the perspective of the quantum formalism, these vector spaces, matrices and scalar in question can be identified as Hilbert spaces, density matrices and complex scalars, respectively.

Completely positive maps

The definition of completely positive maps play an important role in quantum mechanics, since a quantum operations are a completely positive maps. As we will see ahead, the complete positivity condition, ensures a sense of physical reality to these quantum operations.

At first let us define positive maps. A linear map Λ is a positive map if $\Lambda(A) \geq 0$ for every matrix $A \in \mathcal{V}$ that satisfies the positivity condition $A \geq 0$.

So considering another vector space \mathcal{Y} of dimension k , any positive map Λ can be naturally extended to another linear map $\tilde{\Lambda}$ given by

$$\tilde{\Lambda} = Id_k \otimes \Lambda : \mathcal{Y} \otimes \mathcal{V} \rightarrow \mathcal{Y} \otimes \mathcal{W}. \quad (2.15)$$

If $\tilde{\Lambda}$ is positive for every matrix $C \in \mathcal{Y} \otimes \mathcal{V}$, we say that Λ is k -positive. Then if for all $k \in \mathbb{Z}^+$ Λ is k -positive, we say Λ is completely positive (CP) [11]. In other words, a completely positive map is a map which preserves the positivity even if applied only to a subsystem of a whole system.

To illustrate these concepts let us see a map that is positive but is not completely positive: the transpose operation. The transpose operation T on a single qubit ψ is:

$$\psi \rightarrow \psi^T = T(\psi), \quad (2.16)$$

$$\begin{pmatrix} |\alpha|^2 & \alpha\beta^* \\ \alpha^*\beta & |\beta|^2 \end{pmatrix} \rightarrow \begin{pmatrix} |\alpha|^2 & \alpha\beta^* \\ \alpha^*\beta & |\beta|^2 \end{pmatrix}^T = \begin{pmatrix} |\alpha|^2 & \alpha^*\beta \\ \alpha\beta^* & |\beta|^2 \end{pmatrix},$$

where in the matrix representation we used the standard basis $\{|0\rangle, |1\rangle\}$. So $T(\psi)$ certainly preserves both trace and positivity, the result is a density operator. The transpose operation is a positive map $T(\psi) \geq 0$.

Now considering a general pure bipartite state of two qubits $|\psi_{AB}\rangle = \sum_{ij} c_{ij} |i\rangle|j\rangle$ in which density operator is given by

$$\psi = \sum_{ij} c_{ij} c_{kl}^* |i\rangle\langle k| \otimes |j\rangle\langle l|, \quad (2.17)$$

the partial transpose on first qubit A , can be defined as follows:

$$\psi^{TA} \equiv T \otimes \mathbb{1}(\psi) = \sum_{ij,kl} c_{ij} c_{kl}^* (|i\rangle\langle k|)^T \otimes |j\rangle\langle l|. \quad (2.18)$$

Analogously the partial trace on qubit B is $\psi^{TB} = \mathbb{1} \otimes T(\psi)$. Unlike the transpose operation, the partial transpose is not always positive. Take, for example, the partial transpose of the state $\psi = (|00\rangle + |11\rangle)(\langle 00| + \langle 11|)/2$ on the first qubit:

$$\psi = \frac{1}{2} \begin{pmatrix} 1 & 0 & 0 & 1 \\ 0 & 0 & 0 & 0 \\ 0 & 0 & 0 & 0 \\ 1 & 0 & 0 & 1 \end{pmatrix} \rightarrow \psi^{TA} = \frac{1}{2} \begin{pmatrix} 1 & 0 & 0 & 0 \\ 0 & 0 & 1 & 0 \\ 0 & 1 & 0 & 0 \\ 0 & 0 & 0 & 1 \end{pmatrix}$$

ψ^{TA} has a negative eigenvalue and thus doesn't represent a quantum state. So the transpose operation is an example of a positive map $T(\psi) \geq 0$ which is not completely positive.

2.2.2 Defining Quantum Operations

As previously mentioned, the quantum operation formalism is a general tool for describing the transformations that a quantum system can undergo.

Definition: A quantum operation is a completely positive map defined as $\Lambda : \mathcal{H}_1 \rightarrow \mathcal{H}_2$, such that

$$\psi \rightarrow \Lambda(\psi) \quad (2.19)$$

where ψ and $\Lambda(\psi)$ are density operators in Hilbert spaces \mathcal{H}_1 and \mathcal{H}_2 respectively.

As a trivial example, any unitary evolution U must be an admissible quantum operation

$$\psi \rightarrow U\psi U^\dagger = \mathcal{U}(\psi), \quad (2.20)$$

in which $\mathcal{U} : \mathcal{H}_1 \rightarrow \mathcal{H}_1$.

We will now present an elegant way to represent the most general quantum operation, called be the Kraus operators sum representation [31].

Theorem: Let \mathcal{H}_1 and \mathcal{H}_2 Hilbert spaces with dimensions n and m , and a quantum operation $\Lambda : \mathcal{H}_1 \rightarrow \mathcal{H}_2$, then there are a finite set of linear operators $\{K_i\}_{i=1}^{N \leq nm}$ with $K_i : \mathcal{H}_1 \rightarrow \mathcal{H}_2$, such that

$$\Lambda(\psi) = \sum_i^N K_i \psi K_i^\dagger, \quad (2.21)$$

with

$$\sum_i^N K_i^\dagger K_i = id_n. \quad (2.22)$$

The elements $\{K_i\}$ is called Kraus operators.

The relation (2.21) fits the completeness relations that arise from requiring that trace of $\Lambda(\psi)$ to be equal one

$$\text{tr}(\Lambda(\psi)) = \text{tr}\left(\sum_i K_i \psi K_i^\dagger\right) = \text{tr}\left(\sum_i K_i^\dagger K_i \psi\right) = 1, \quad (2.23)$$

once this relation is true for all density matrices ψ . Quantum operations that satisfy this condition are called trace-preserving.

2.2.3 Coarse Graining Channel

In this section we will show a quantum operation that plays a crucial role in this work, called: Coarse Graining channel. In general Coarse-grained models aim at describing the behavior of complex systems using an simplified representation in which preserve the properties of the system that we have access. In other words, complex systems are represented by adequate simplified representation with less degrees of freedom that facilitates the study of the system.

In a quantum mechanical approach, the coarse graining is a quantum operation that can be defined as

Definition: A completely positive map $\Lambda_{CG} : \mathcal{H}_D \rightarrow \mathcal{H}_d$ is a coarse graining operation if and only if $\dim(\mathcal{H}_D) > \dim(\mathcal{H}_d)$.

From this general definition, through this work we will explore some useful applications for coarse graining operations.

A Blurred Detector

As an introduction to what will follow, here we will present the main idea about the coarse graining model that will be used in the next chapter. Consider the follow experimental situation: imagine that we want to measure the information of a number of neighboring atoms in a lattice, but our detecting device doesn't have enough resolution to resolve the light coming from each individual atom. To describe this situation we can construct a coarse graining model in such way that we take the information of these multiple unsolved signals as a single effective one coming from one atom in a coarse-grained level (such situation is pictorially illustrated in Figure 2.1).

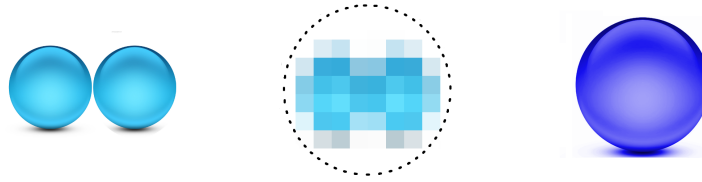


FIGURE 2.1: **A pictorially scheme of coarse graining model.** In the left the two spheres that represent a composite system of two atoms. In the middle we have the blurred detection of the system. Then in the third picture we approximate the blurred signal as a single one related to a single atom in a coarse graining level.

Bringing this situation to the scenario of quantum information, we can identify each atom as a two level quantum system. In this way a system of n atoms is described by a D -dimensional state $\psi \in \mathcal{H}_D$, with $D = 2^n$. So we want to construct a coarse graining map $\Lambda_{CG}^{n \rightarrow 1} : \mathcal{H}_D \rightarrow \mathcal{H}_2$ such that take a system of n atoms to an effective coarse graining level of a single atom.

The simplest case, where our detector can not resolve two neighboring atoms, the resulting signal can be related to a single atom in a coarse-grained level. Such situation is described by a coarse graining map $\Lambda_{CG}^{2 \rightarrow 1} : \mathcal{H}_4 \rightarrow \mathcal{H}_2$. So through a composition of $\Lambda_{CG}^{2 \rightarrow 1}$, coarse graining maps of higher dimensional cases can be achieved, like $\Lambda_{CG}^{4 \rightarrow 1} : \mathcal{H}_{16} \rightarrow \mathcal{H}_2$ and $\Lambda_{CG}^{8 \rightarrow 1} : \mathcal{H}_{256} \rightarrow \mathcal{H}_2$:

$$\begin{aligned} \Lambda_{CG}^{4 \rightarrow 1} &= \Lambda_{CG}^{2 \rightarrow 1} \circ (\Lambda_{CG}^{2 \rightarrow 1} \otimes \Lambda_{CG}^{2 \rightarrow 1}), \\ \Lambda_{CG}^{8 \rightarrow 1} &= \Lambda_{CG}^{2 \rightarrow 1} \circ (\Lambda_{CG}^{2 \rightarrow 1} \otimes \Lambda_{CG}^{2 \rightarrow 1}) \circ (\Lambda_{CG}^{2 \rightarrow 1} \otimes \Lambda_{CG}^{2 \rightarrow 1} \otimes \Lambda_{CG}^{2 \rightarrow 1} \otimes \Lambda_{CG}^{2 \rightarrow 1}), \end{aligned} \quad (2.24)$$

where "o" denotes composition of maps. This process are schematically represented in the Figure 2.2.

This approach will play an important role in the next chapter. There we will describe an experimental realization with strong correlated cold bosonic atoms in an optical lattice. This set up is an ideal quantum spin system where we can investigate the dynamics of the entanglement among its constituents. In this way the coarse graining approach that we started to construct here will allows us to investigate this entanglement dynamics at coarse graining levels.

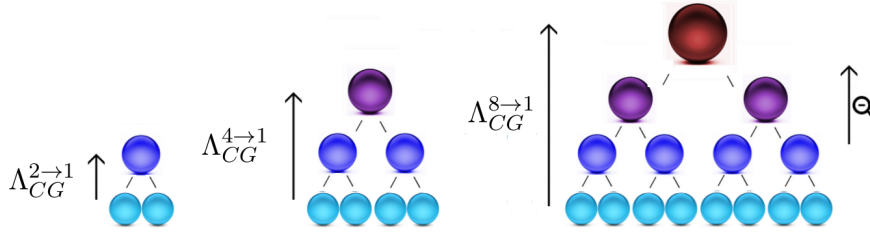


FIGURE 2.2: From a composition of $\Lambda_{CG}^{2 \rightarrow 1}$, higher dimensional coarse graining operations $\Lambda_{CG}^{4 \rightarrow 1}$ and $\Lambda_{CG}^{8 \rightarrow 1}$ can be defined.

2.3 Entangled States

Quantum composite systems display a property that is unknown for classical ones, this feature is called entanglement. As we shall see in this section, because of the entanglement between the constituents of a system, each particle of the system can not be independently described from the others, we have only the information of the system as a whole.

We will show how entanglement is characterized in pure and mixed states. Besides we will discuss possible ways of distinguishing entangled states from non-entangled states, and also ways to quantify the entanglement.

2.3.1 Entangled Pure States

Definition: Given an pure state $|\Psi\rangle \in \mathcal{H}_A \otimes \mathcal{H}_B$, we say it is separable if there exists $|\psi_A\rangle \in \mathcal{H}_A$ and $|\psi_B\rangle \in \mathcal{H}_B$ such that $|\psi\rangle = |\psi_A\rangle \otimes |\psi_B\rangle$. Otherwise the state $|\psi\rangle$ is entangled.

As an examples of separable pure states we have $\{|0\rangle \otimes |0\rangle; |0\rangle \otimes |1\rangle; |1\rangle \otimes |0\rangle; |1\rangle \otimes |1\rangle\}$ and as an example of entangled pure states we have the so called Bell's states:

$$|\phi^\pm\rangle = \frac{(|00\rangle \pm |11\rangle)}{\sqrt{2}} \quad \text{and} \quad |\psi^\pm\rangle = \frac{(|01\rangle \pm |10\rangle)}{\sqrt{2}}. \quad (2.25)$$

We will see in the following sections, when we talk about detection and quantification of entanglement that the Bell states are maximally entangled states.

2.3.2 Entangled Mixed States

Analogously from the definition of entanglement for pure states, we can extend the concept of entanglement to mixed states.

Definition: A mixed state $\psi \in \mathcal{H}_A \otimes \mathcal{H}_B$ is separable if there exist local states $(\psi_A)_i \in \mathcal{H}_A$, $(\psi_B)_i \in \mathcal{H}_B$ and non-negative weights p_i such that ψ can be expressed as a convex sum $\psi = \sum_i p_i (\psi_A)_i \otimes (\psi_B)_i$.

2.4 Separability Criteria

As already discussed, the separability of a given state is defined by the existence of a decomposition: into product of pure states, or into a convex sum of tensor product for mixed states. Nevertheless the failure to find a decomposition of a state does not necessarily identify it as entangled. Perhaps the state is separable but the appropriate decomposition could not be identified.

We show that for pure states, using a useful tool called Schmidt decomposition, we can easily derive a general separability criteria. However, for mixed states, only for low-dimensional systems (2×2 and 2×3) a similar separability criteria can be easily evaluated. This criteria is on positiveness of the transpose operation.

2.4.1 Pure States

There are many ways of expressing a separable state into a tensor product of two states. However there is a particular decomposition that is very useful to entanglement characterization, called Schmidt decomposition.

Schmidt decomposition

The Schmidt decomposition is characterized by the following theorem

Theorem: Let \mathcal{H}_A and \mathcal{H}_B be Hilbert spaces with dimensions m and n with $m \leq n$. For every state $|\Psi\rangle \in \mathcal{H}_A \otimes \mathcal{H}_B$ there are bases $\{|u_i\rangle\} \in \mathcal{H}_A$ and $\{|v_i\rangle\} \in \mathcal{H}_B$ such that $|\Psi\rangle$ can be written in the form

$$|\Psi\rangle = \sum_{i=0}^{m-1} \sqrt{\lambda_i} |u_i\rangle \otimes |v_i\rangle, \quad (2.26)$$

where the λ_i 's are non-negative real numbers.

The proof of this theorem is quite simple. Let \mathcal{H}_A and \mathcal{H}_B , be Hilbert spaces with dimensions m and n with $m \leq n$. An arbitrary bipartite pure state $|\Psi\rangle \in \mathcal{H}_A \otimes \mathcal{H}_B$ is given by

$$|\Psi\rangle = \sum_{i=0}^{m-1} \sum_{j=0}^{n-1} c_{ij} |i\rangle |j\rangle, \quad (2.27)$$

where $\{|i\rangle\}$ and $\{|j\rangle\}$ are arbitrary local bases in \mathcal{H}_A and \mathcal{H}_B respectively. By singular value decomposition [19], the matrix coefficient of (2.27) given by

$$C = \sum_{i=0}^{m-1} \sum_{j=0}^{n-1} c_{ij} |i\rangle \langle j| \quad (2.28)$$

can be decomposed as follows

$$C_{m \times n} = U_{m \times m} S_{m \times n} V_{n \times n}^\dagger, \quad (2.29)$$

where $U = \sum_{i,j=0}^{m-1} u_{ij}|i\rangle\langle j|$ and $V = \sum_{i,j=0}^{n-1} v_{ij}|i\rangle\langle j|$ are unitary matrices and $S = \sum_{i=0}^{m-1} s_i|i\rangle\langle i|$ is a diagonal matrix whose diagonal elements $\{s_0, s_1, \dots, s_{m-1}\}$ are non-negative real numbers. The elements $\{s_k\}$ are called singular values of C . Then we can write the matrix elements c_{ij} of (2.28) by

$$c_{ij} = \sum_{k=0}^{m-1} u_{ik}s_k v_{jk}^* = \sum_{k=0}^{m-1} \langle i|U|k\rangle s_k \langle j|V^*|k\rangle. \quad (2.30)$$

Like eigenvalues of a matrix, also the singular values $\{s_k\}$ are uniquely defined.

Rewriting (2.27) by inserting (2.30) and defining the Schmidt coefficients of $|\Psi\rangle$ by $\lambda_k \equiv s_k^2$, we have

$$\begin{aligned} |\Psi\rangle &= \sum_{i=0}^{m-1} \sum_{j=0}^{n-1} \left(\sum_{k=0}^{m-1} \langle i|U|k\rangle \sqrt{\lambda_k} \langle j|V^*|k\rangle \right) |i\rangle|j\rangle \\ &= \sum_{k=0}^{m-1} \sqrt{\lambda_k} \left(\sum_{i=0}^{m-1} |i\rangle\langle i|U|k\rangle \right) \left(\sum_{j=0}^{n-1} |j\rangle\langle j|V^*|k\rangle \right) \\ &= U \otimes V^* \sum_{k=0}^{m-1} \sqrt{\lambda_k} |k\rangle|k\rangle \end{aligned} \quad (2.31)$$

where in the second line we used $\sum_i |i\rangle\langle i| = \mathbb{1}$. Also we can rewrite (2.31) defining a new basis by the following transformations $U|k\rangle = |u_k\rangle$ and $V|k\rangle = |v_k\rangle$:

$$|\Psi\rangle = \sum_{k=0}^{m-1} \sqrt{\lambda_k} |u_k\rangle|v_k\rangle. \quad (2.32)$$

It is important to note that, since s_k are unique, for any state $|\Psi\rangle$ its Schmidt coefficients values also are uniquely defined.

From the Schmidt coefficients of a pure state $|\Psi\rangle$ there is an easy way to decide about its separability. Once the Schmidt basis is given by separable states $\{|u_k\rangle|v_k\rangle\}$, if there is only one non-vanishing λ_k , then the state $|\Psi\rangle$ can be expressed in the form (2.27), and then the state is separable. Otherwise, if there are at least two non-vanishing λ_k the state $|\Psi\rangle$ is entangled.

2.4.2 Mixed States

Unlike pure states, for mixed states does not exist an elegant criterion for separability. In general, this is due to the fact that the degree of mixing of the reduced density matrices related to the mixed state are not an indicator of entanglement. Usually, separability criteria for bipartite mixed states are feasible only for low-dimensional systems.

In the following we will show a separability criterion for bipartite systems known as Peres-Horodecki criterion. It consists of a necessary condition for separability of an arbitrary bipartite system.

Positive Maps

Positive quantum maps like $\Lambda_P : \mathcal{H}_B \mapsto \mathcal{H}_A$ can be used to find a necessary condition of separability in bipartite systems [10]. We can extend this

positive map on $\mathcal{H} = \mathcal{H}_A \otimes \mathcal{H}_B$ locally acting in the second subsystem by $\mathbb{1} \otimes \Lambda_P$. However, there are states $\psi \in \mathcal{H}_1 \otimes \mathcal{H}_2$, such that, for some maps Λ_P , $\mathbb{1} \otimes \Lambda_P$ is not a positive operator. Given a separable state

$$\psi = \sum_i p_i (\psi_A)_i \otimes (\psi_B)_i \quad (2.33)$$

so, applying the extended map

$$(\mathbb{1} \otimes \Lambda_P)(\psi) = \sum_i p_i (\psi_A)_i \otimes \Lambda_P((\psi_B)_i). \quad (2.34)$$

Since

$$p_i, (\psi_A)_i, \Lambda_P((\psi_B)_i) \geq 0,$$

$(\mathbb{1} \otimes \Lambda_P)(\psi)$ remains a positive operator. So we can conclude that ψ is entangled if we can find a positive map Λ_P such that $(\mathbb{1} \otimes \Lambda_P)(\psi)$ has at least one negative eigenvalue. Moreover, since $(\mathbb{1} \otimes \Lambda_P)(\psi) \in \mathcal{H}_A \otimes \mathcal{H}_A$, a state ψ is separable if and only if $(\mathbb{1} \otimes \Lambda_P)(\psi) \geq 0$ for all positive maps $\Lambda_P : \mathcal{H}_B \mapsto \mathcal{H}_A$. But, such maps provide only a necessary condition for separability. That is, if we fail to find a map Λ_P , such that $(\mathbb{1} \otimes \Lambda_P)$ is not a positive operator, we cannot immediately conclude that ψ is separable, since we may have failed to check all possible maps Λ_P .

Peres-Horodecki criterion

The Peres-Horodecki criterion, also called PPT-criterion, gives a necessary condition for separability of states in bipartite systems. We will use the transpose and partial transpose operations, saw in (2.16) and (2.18). We already know that the transpose operation is positive $T(\psi) \geq 0$ but not necessarily $\mathbb{1} \otimes T(\psi)$ is, since $\mathbb{1} \otimes T$ is not a positive map. Then for every pure state $\mathbb{1} \otimes T(\psi) \geq 0$, and is called PPT (positive partial transpose). However the PPT-criterion is only a necessary separability criterion, once there are entangled states that $\mathbb{1} \otimes T \geq 0$.

The PPT-criterion becomes both necessary and sufficient if we restrict the dimension of the system to 2×2 or 2×3 . The underlying reason for this is that any positive map $\Lambda_P : \mathbb{C}^2 \mapsto \mathbb{C}^2$ or $\Lambda_P : \mathbb{C}^2 \mapsto \mathbb{C}^3$ can be written as

$$\Lambda_P = \Lambda_{CP}^{(1)} + \Lambda_{CP}^{(2)} \circ T, \quad (2.35)$$

where Λ_{CP} are completely positive maps [23]. Then the condition $(\mathbb{1} \otimes \Lambda_P)(\psi) \geq 0$ reduces to

$$\begin{aligned} (\mathbb{1} \otimes \Lambda_P)(\psi) &= (\mathbb{1} \otimes \Lambda_{CP}^{(1)})(\psi) + (\mathbb{1} \otimes \Lambda_{CP}^{(2)})(\mathbb{1} \otimes T)(\psi) \\ &= (\mathbb{1} \otimes \Lambda_{CP}^{(1)})(\psi) + (\mathbb{1} \otimes \Lambda_{CP}^{(2)})(\psi^{T_B}) \geq 0, \end{aligned} \quad (2.36)$$

where T_B is the partial transposition of ψ related to the second subsystem. In the above equation, the extended maps $\mathbb{1} \otimes \Lambda_{CP}^{(1,2)}$ are positive maps, since $\Lambda_{CP}^{(1,2)}$ are completely positive, thus $(\mathbb{1} \otimes \Lambda_{CP}^{(1)})(\psi)$ have only non-negative eigenvalues. And likewise a general dimensional case seen above, if ψ is such that $\mathbb{1} \otimes T(\psi) \geq 0$, then $(\mathbb{1} \otimes \Lambda_{CP}^{(2)})(\psi^{T_B}) \geq 0$. This implies that $(\mathbb{1} \otimes \Lambda_P)(\psi) \geq 0$ for any positive map Λ_P , since the negative eigenvalues

in these dimensions come from the transposition map. In this condition, ψ is separable. And otherwise, ψ is entangled if $\mathbb{1} \otimes T(\psi)$ has at least one negative eigenvalue. Then we found a necessary and sufficient separability condition for 2×2 and 2×3 bipartite systems.

2.5 Entanglement Monotones and Measures

In our study of quantum entanglement, in summary, we already defined entangled states and listed some useful tools to check on the separability of quantum states. Concluding our approach, in this section we are interested in quantifying the entanglement. We will introduce some of the most well known entanglement measures: Entanglement entropy, concurrence and Negativity. These quantities allow us to compare the amount of entangled between different states.

The definition of an entanglement measure is a difficult task. Given the importance of the problem, there are many proposes about entanglement measures. We will present some quantifiers proposals based on an axiomatic definition [4]. That is, functions that satisfy some reasonable postulates, and as such can be considered an entanglement quantifier.

At first, we will classify all operations that one could apply to a composite quantum system, in a way that no entanglement is generated. This is known as "entanglement resource theory". Once this is done, one can take the decrease of correlations under all such operations a defining property of measure on entanglement. These operations are classified as local operations and classical communication (LOCC).

2.5.1 Local Operations and Classical Communication (LOCC)

Consider a state ψ . The most general operations that acts only on the second subsystem is given by

$$\psi \rightarrow \sum_i (\mathbb{1} \otimes \epsilon_i) \psi (\mathbb{1} \otimes \epsilon_i^\dagger) \quad (2.37)$$

in which $\sum_i \epsilon_i^\dagger \epsilon_i = \mathbb{1}$. This operation does not induce any correlations, since

$$\psi = \psi_A \otimes \psi_B \rightarrow \psi_A \otimes \left(\sum_i \epsilon_i \psi_B \epsilon_i^\dagger \right) \quad (2.38)$$

and

$$\psi = \sum_i p_i (\psi_A)_i \otimes (\psi_B)_i \rightarrow \sum_i p_i (\psi_A)_i \otimes \left(\sum_j \epsilon_j (\psi_B)_i \epsilon_j^\dagger \right) \quad (2.39)$$

Analogously this procedure can be done performing a general operation on first subsystem.

Now let us increase correlations by application of local operations that depends on the outcomes of previous operations:

$$\begin{aligned}
\psi &\rightarrow \sum_i (\mathbb{1} \otimes \epsilon_i) \psi (\mathbb{1} \otimes \epsilon_i^\dagger) \\
&\rightarrow \sum_{ij} (\zeta_{ij} \otimes \mathbb{1}) (\mathbb{1} \otimes \epsilon_i) \psi (\mathbb{1} \otimes \epsilon_i^\dagger) (\zeta_{ij}^\dagger \otimes \mathbb{1}) \\
&\vdots \\
&\rightarrow \sum_{ij\dots k} (\mathbb{1} \otimes \Phi_{ij\dots k}) \cdots (\zeta_{ij} \otimes \mathbb{1}) (\mathbb{1} \otimes \epsilon_i) \psi (\mathbb{1} \otimes \epsilon_i^\dagger) (\zeta_{ij}^\dagger \otimes \mathbb{1}) \cdots (\mathbb{1} \otimes \Phi_{ij\dots k}^\dagger)
\end{aligned} \tag{2.40}$$

Such operations are called local operations and classical communication (LOCC). We call "classical communication" the communication between subsystems in order to know the preceding outcome associated with measurement on the first subsystem, to thereby perform the measurement on the second subsystem. Therefore LOCC operations cannot create entanglement. So, it is reasonable that a potential quantifier of entanglement must be monotone under LOCC. That is a quantity that does not increase under LOCC.

Invariance of Entanglement Under Local Unitaries

In general, it is difficult to verify the monotonicity under LOCC. An easy alternative necessary condition for monotonicity can be derived from unitary operations.

Among all LOCC operations, the local unitary operation

$$\psi \rightarrow U_1 \otimes U_2 \psi U_1^\dagger \otimes U_2^\dagger \tag{2.41}$$

has an inverse that is again LOCC. Thus if we initially apply some local unitary on an arbitrary state ψ , and immediately after applies your inverse, we expect a monotone \mathcal{M} cannot increase after either step

$$\mathcal{M}(\psi) \geq \mathcal{M}(U_1 \otimes U_2 \psi U_1^\dagger \otimes U_2^\dagger) \geq \mathcal{M}(\psi), \tag{2.42}$$

so

$$\mathcal{M}(\psi) = \mathcal{M}(U_1 \otimes U_2 \psi U_1^\dagger \otimes U_2^\dagger). \tag{2.43}$$

Thus we conclude that every entanglement monotone is also invariant under local unitaries. In general, it is difficult to verify the monotonicity, the necessary condition of invariance under local unitaries becomes an easier alternative way to test a potential quantifier of entanglement.

2.5.2 Entanglement Measures

We already saw that a potential entanglement quantifier must be monotone under LOCC (and consequently invariant under local unitaries). However, there are additional important requirements that qualify a monotone as an entanglement measure. The most relevant are [4]:

- **Convexity:** Given two states $\psi_1 \in \mathcal{H}_A \otimes \mathcal{H}_B$ and $\psi_2 \in \mathcal{H}_A \otimes \mathcal{H}_B$, an entanglement monotone \mathcal{M} must be convex in $\mathcal{H}_A \otimes \mathcal{H}_B$

$$\mathcal{M}(p\psi_1 + (1-p)\psi_2) \leq p\mathcal{M}(\psi_1) + (1-p)\mathcal{M}(\psi_2)$$

where $0 \leq p \leq 1$. This implies a probabilistic mix between these states ($p\psi_1 + (1-p)\psi_2$) cannot increase entanglement.

- **Additivity:** For n copies of a state $\psi \in \mathcal{H}$, it is equivalent to assume a single n -fold state $\psi^{\otimes n} \in \mathcal{H}^{\otimes n}$. So an entanglement monotone that fulfills

$$\mathcal{M}(\psi^{\otimes n}) = n\mathcal{M}(\psi)$$

is called additive.

- **Subadditivity:** given two states ψ_1 and ψ_2 in \mathcal{H} for arbitrary two systems. An entanglement monotone that fulfills the inequality

$$\mathcal{M}(\psi_1 \otimes \psi_2) \leq \mathcal{M}(\psi_1) + \mathcal{M}(\psi_2)$$

is called subadditive. This implies that the product state $\psi_1 \otimes \psi_2$ cannot increase entanglement.

Once listed some general properties of entanglement quantifiers. We will show the most frequently used quantifiers in the literature: Entanglement entropy, concurrence and negativity.

Entanglement Entropy

Entanglement entropy is an entanglement quantifier suitable for bipartite pure states. Initially let us define Von Neumann entropy, for arbitrary state $\psi \in \mathcal{H}$ with $\dim(\mathcal{H}) = N$

$$\mathcal{S}(\psi) = -\text{tr}(\psi \ln \psi) = -\sum_i \lambda_i \ln \lambda_i \quad (2.44)$$

where λ_i are the eigenvalues of ψ . This quantity is useful to characterize the state in the sense of

- $\mathcal{S}(\psi) = 0$, if only if ψ is a pure state
- $\mathcal{S}(\psi) = \ln N$, for a maximally mixed state $\frac{\mathbb{1}}{N}$

Now let us look at the situation for a bipartite pure state $\psi \in \mathcal{H}_A \otimes \mathcal{H}_B$. The state ψ is entangled if its reduced matrices are mixed, while ψ is separable if its reduced matrices are pure. Then it is reasonable to think that the level of lack of information for one of the subsystems is a good measure for entanglement in the pair. Then the entanglement entropy $\mathcal{S}E(\psi)$ is defined in terms of Von Neumann entropy of reduced density matrices of ψ

$$\mathcal{S}E(\psi) = \mathcal{S}(\psi_x) = -\text{tr}\psi_x \ln \psi_x = -\sum_i \lambda_i \ln \lambda_i \quad (2.45)$$

with x referring to either first or second subsystem and λ_i are the eigenvalues of ψ_x . The values of $\mathcal{S}E(\psi_x)$ have the following meanings

- $S_E(\psi_x) = 0$ if only if ψ is a product state, and thus separable;
- $S_E(\psi_x) = N$ for a maximally entanglement.

Concurrence

From Von Neumann entropy we can derive another measure of mixedness in quantum states. By taking the Mercator series with first order approximation $\ln(x) \approx x - 1$ (with $|x - 1| < 1$), (2.44) become:

$$\mathcal{S}(\psi) \approx \text{tr}(\psi(\psi - 1)) = 1 - \text{tr}\psi^2 \quad (2.46)$$

Then we define the linear entropy $\mathcal{S}_L(\psi)$ for a d -dimensional system as [ref]

$$\mathcal{S}_L(\psi) = \frac{d}{d-1}(1 - \text{tr}\psi^2) \quad (2.47)$$

where $\mathcal{S}_L(\psi) = 0$ if only if ψ is a pure state and $\mathcal{S}_L(\psi) = 1$ for a maximally mixed state. As we will see, this equation is quite useful for algebraic manipulations.

In the same way that we have defined entanglement entropy \mathcal{S}_E from Von Neumann entropy \mathcal{S} , now in terms of lineal entropy \mathcal{S}_L we derive another entanglement measure, the concurrence \mathcal{C} [22, 47]. Considering a two dimensional system we have $\mathcal{S}_L(\psi) = 2(1 - \text{tr}\psi^2)$. So, taking the square root we define the concurrence for bipartite pure state of arbitrary dimension:

$$\mathcal{C}(|\psi\rangle) = \sqrt{2(1 - \text{tr}\psi_x^2)} \quad (2.48)$$

where ψ_x is the reduced density matrix with x refers to either first or second subsystem. An alternative form can be reached in terms of Schmidt coefficients, since $\text{tr}\psi_x^2 = \sum_i \lambda_i^2$ and $1 = (\sum_j \lambda_j)^2$, (2.48) become

$$\mathcal{C}(|\Psi\rangle) = 2 \sqrt{\sum_{i < j} \lambda_i \lambda_j} \quad (2.49)$$

so the concurrence can be given by the square root of the product of two different Schmidt coefficients.

The concurrence can be extended over mixed states. It is done by an optimal decomposition of the mixed state ψ that give the lowest average concurrence:

$$\mathcal{C}(\psi) = \inf_{\{p_i, |\psi_i\rangle\}} \sum_i p_i \mathcal{C}(|\psi_i\rangle) \quad \text{with} \quad \psi = \sum_i p_i |\psi_i\rangle \langle \psi_i| \quad (2.50)$$

this definition ensure the convexity of the entanglement measure. However for high dimensional system this optimization is quite difficult to achieve. Actually, analytical expressions are only known for states of high symmetry and for two qubits systems in which the minimum is obtained by:

$$\mathcal{C}(\psi) = \max\{0, \sqrt{a_1} - \sqrt{a_2} - \sqrt{a_3} - \sqrt{a_4}\} \quad (2.51)$$

$\{a_i\}$ are the eigenvalues of the matrix R , arranged in decreasing order, where R is

$$R = \psi(\sigma_y \otimes \sigma_y)\psi^*(\sigma_y \otimes \sigma_y) \quad (2.52)$$

with σ_y is the Pauli matrix.

Negativity

Another frequently used monotone is negativity \mathcal{N} [45]. Previously we saw that given a state ψ , if its partial transpose ψ^{TB} has at least one negative eigenvalue, ψ is entangled. Based on this result follows the definition

$$\mathcal{N}(\psi) = \frac{\|\psi^{TB}\|_1 - 1}{2} \quad (2.53)$$

where $\|A\|_1 = \text{tr}\sqrt{(A)^\dagger A}$ is the trace norm. So

- $N = 0$ if ψ^{TA} is positive semi-definite ($\psi^{TA} \geq 0$)
- $N > 0$ if ψ^{TA} has at least one negative eigenvalue

Therefore, as well for the PPT-criterion, negativity is completely trustworthy only for 2×2 or 2×3 systems, since there are entangled states with $\psi^{TB} \geq 0$ in high dimensional systems.

Chapter 3

Spin-Entanglement in a Coarse-Grained Optical Lattice

Currently quantum many-body systems is one of the more productive field in quantum physics. Especially in strongly correlated regimes, the role of entanglement among their constituents is crucial for quantitative description of the quantum many-body systems. In addition, entanglement is one of the resources for quantum information [5] so that its microscopic control is needed for the main applications.

Since entanglement is intrinsically fragile against the action of the environment, the microscopic control of quantum entangled system, becomes a great experimental challenge. So, currently there are few well-controlled physical systems that offer the possibility of exploring many body entanglement. A prominent one is spin systems realized with ultracold atoms in optical lattices [9]. In this framework recent works accomplished a single site detection of spin-entanglement in a Bose-Hubbard chain [18].

However this experimental realizations spend expensive experimental resources. In special, for single site detection in optical lattices [39] the need for high accurate equipments, like high-resolution microscopy, can become an obstacle. In order to make the experimental procedure simpler and more feasible, a question arises: Given an entangled spin-system, is it possible to have a satisfactory description of the spin-entanglement if we are not able to fully resolve the system?

In order to answer this question, in this chapter we will develop a suitable proposal. Simulating a detector with insufficient resolution, we will take the information from a number of neighboring sites of the lattice as a single site. Such procedure allows us to describe the entanglement behavior taking into account different ranges of resolution of the spin chain.

In the first part of this chapter we will report an overview about the already mentioned experimental achievement [18], highlighting the main results that are interesting to us. Finally, in the second part, we will present a coarse graining view of spin-entanglement dynamics in a Bose-Hubbard chain. By applying the proposed coarse graining map, we will be able to compare the loss of information about the entanglement dynamics in different degrees of the lattice sharpness.

3.1 Spin-entanglement Dynamics in a Bose-Hubbard Chain

The work [18] was a remarkable experimental realization in the field of many body quantum mechanics. From confined ultracold atoms in an optical lattice, the researchers were able to measure entanglement between spins of atoms located on two lattice sites in a 1D Bose-Hubbard chain. From an initially spin-impurity atom in the center of the chain, an outwards propagating entanglement wave could be observed.

Focusing in the main aspects, in following sections we will present an brief overview about the above experimental achievement. Before actually describing the experimental procedure performed in [18], let us get some preliminary knowledge about the creation of optical lattices, and how manipulate ultracold atoms in there. This basic description allows us, in sequence, to appropriately describe the realization [18]. Since the purpose is only to provide a general picture of the main experimental features found in [18], if necessary, references for a more detailed and technical description will be given.

3.1.1 Storing Atoms in Optical Lattice

Ultracold atoms in optical lattices are the background physical system that supports the experimental procedure to be described [18]. Way beyond entanglement measurement, ultracold bosonic and fermionic gases in optical lattices represent an interdisciplinary field that has been explored for a wide variety of problems: from probing fundamental condensed-matter physics problems [15, 20, 32, 34], up to applications in quantum optics and quantum information processing [8], passing by the study of atomic and molecular physics [35, 38].

This high range of applications that ultracold atoms in optical lattice offer is due to its high level of control, which can be adjusted in very different ways.

Light-atom interaction

Optical lattices are created by counter-propagating lasers beams applied on an ultracold atomic gas . The counter-propagating lights generate a standing wave, which in turn interacts with the neutral atoms, creating a periodic dipole potential (Figure 3.1).

In a general light-atom interaction there are both a dissipative and a conservative part. The dissipative one relates to the absorption of the photons and the following spontaneous emission. However the light frequency ω_L used in optical lattices is tuned far away from the atomic resonance ω_0 , such that the atomic excitation can be neglected. So arises in the atom a purely conservative induced dipole moment \mathbf{d} , given by [25]

$$\mathbf{d} = \alpha(\omega_L)\mathbf{E}(\mathbf{r}), \quad (3.1)$$

where $\mathbf{E}(\mathbf{r})$ is the electric field amplitude at position \mathbf{r} , ω_L is the light frequency and $\alpha(\omega_L)$ is the complex polarizability of the atom.

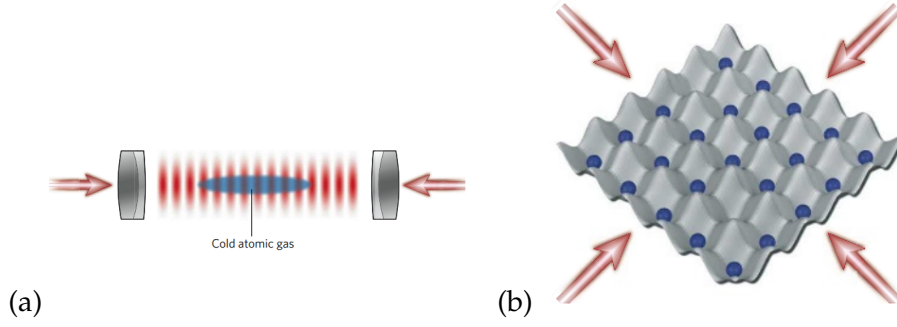


FIGURE 3.1: Creation of an optical lattice. (a) counter-propagating laser beams create a standing wave that acts as microscopic trap for the atoms (b) Combining more laser beams it is possible to create a higher-dimensional lattice, such the 2D lattice shown. Adapted with permission from [7]

At the same time that the electric field induces a dipole moment in the atom, it interacts with the moment, creating a trapping potential $V_{dip}(\mathbf{r})$ for the atoms [9]:

$$V_{dip}(\mathbf{r}) = -\mathbf{d} \cdot \mathbf{E}(\mathbf{r}) \approx \alpha(\omega_L) |\mathbf{E}(\mathbf{r})|^2 \quad (3.2)$$

with the term $|\mathbf{E}(\mathbf{r})|^2$ related to the intensity of the laser light field:

$$I(\mathbf{r}) = \frac{c\epsilon_0}{2} |\mathbf{E}(\mathbf{r})|^2, \quad (3.3)$$

where c is the speed of light, and ϵ_0 is the permittivity. The trapping potential (3.2) can be attractive if $\omega_L \ll \omega_0$ (the atoms are captured in the intensity maximum) or repulsive if $\omega_L \gg \omega_0$ (the atoms are captured in the intensity minimum).

Therefore a 1D periodic potential can then be formed simply by interfering two counter-propagating laser beams (with wavelength λ_L) that forms an optical standing wave with period $\lambda_L/2$. Hence generating an optical lattice with lattice spacing $a_{lat} = \lambda_L/2$ that trap the atoms. The 1D potential trap is given by [9]

$$V_{lat}(x) = V_0 \sin^2(k_L x) \quad (3.4)$$

where $k_L = 2\pi/\lambda_L$ is the wave vector of the laser light and V_0 the potential depth, see Figure 3.2. The potential depth V_0 usually is given in units of the recoil energy $E_R = \hbar^2 k_L^2 / 2m = \hbar^2 / 8ma_{lat}^2$, in which m is the mass of the single neutral atom. The recoil energy E_R is the natural energy scale for neutral atoms in periodic light fields.

Overlapping more laser beams, one can obtain 2D and 3D periodic potentials. A simplest 3D potential trap has the approximate form (see [21] and references therein)

$$V_{lat}(x, y, z) = V_x \sin^2(k_L x) + V_y \sin^2(k_L y) + V_z \sin^2(k_L z). \quad (3.5)$$

A schematic illustration of lattice geometries are shown in the Figure 3.3.

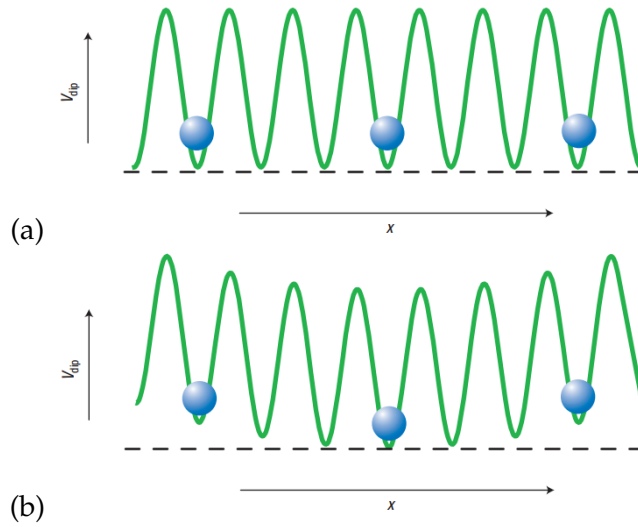


FIGURE 3.2: 1D optical lattice potential. (a) A periodic potential related to the light standing wave trap the atoms (b) Actually the potential are inhomogeneous, this is due of the residual harmonic trap associated to the gaussian beam profile of the laser, which overlaps the periodic potential [9]. (b) Since is an weak residual potential, in the center of the sample the periodic potential can be approximate to homogeneous. Adapted with permission from [9]

Bose-Hubbard Systems

In summary, the Bose-Hubbard model is used to describe interacting particles in a lattice. This model is described by a Hamiltonian consisting of two principal terms: a kinetic term, allowing for tunneling of particles between sites of the lattice and a potential term, consisting of on-site interaction. The (single band) Bose-Hubbard Hamiltonian is given by [15]:

$$\hat{H}_{BH} = -J \sum_j \hat{a}_j^\dagger \hat{a}_{j+1} + \sum_j \frac{U}{2} \hat{n}_j (\hat{n}_j - 1) + \sum_j \epsilon_j \hat{n}_j \quad (3.6)$$

where index j refer to spin site in the chain. The first term is the kinetic term, with J the single-particle tunneling rate and \hat{a}_j^\dagger (\hat{a}_j) is the raising (lowering) operator for site j . The second term relates to potential energy, where U denotes on-site interaction energy and \hat{n}_j is the number operator. Finally, the third term represents an external confinement with $\epsilon_j = V_{ext}(x_j)$ that describes an energy offset of each lattice site (for homogeneous systems ϵ_j is constant).

Ultracold atoms in an optical lattice are mapped onto the Bose-Hubbard model (3.6) when the atoms in the lattice are in a sufficiently low temperature, such that any long-range-interaction can be ignored. In an experimental realization, the parameters J and U in (3.6) can be easily handled by the experimentalist, since they are directly related to the potential depth of the optical lattice. Decreasing the potential depth, the tunneling barrier between lattice sites is decreased and consequently the tunneling rate J increase. On the other hand in a deeper lattice, the greater confinement of the wave function results in an increase of on-site interaction U . Therefore, the

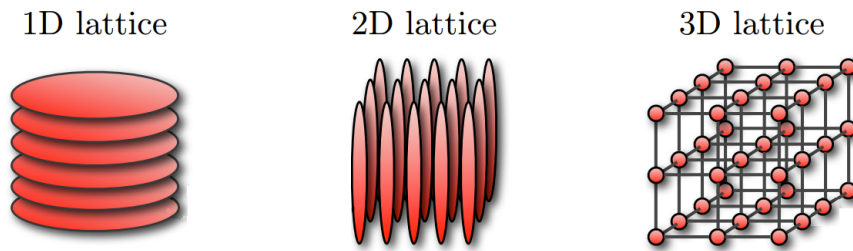


FIGURE 3.3: Schematics of an 1D, 2D and 3D optical lattices. Superimposing one, two or three orthogonal 1D potential lead to diverse optical lattice geometries. Adapted with permission from [16]

ratio U/J can be easily adjusted basically by changing the intensity of the counter-propagating laser beams that make up the lattice.

Superfluid to Mott insulator Phase Transition

A diluted ultracold gas loaded in an optical lattice that can be described by (3.6), may assume the superfluid state or the Mott insulating state [20]. In the regime of weak interactions relative to the kinetic energy $U/J \ll 1$, the system exhibit superfluid state, in which each atom is delocalized over the lattice. In this case the whole system is described by a matter wave, Figure 3.4a, and the atom number per lattice site follows a poissonian distribution. On the other hand, for the regime of strong interactions $U/J \gg 1$, the system become strongly correlated entering in the Mott insulator state. The atoms are localized to single lattice sites, with a fixed particle number. Now, perfect correlations in the particle number per site exist and the system can no longer be described by a matter wave, Figure 3.4b.

As previously discussed, the experimentalist can continuously adjust the ratio U/J through changing the strength potential. In fact the implementation of the quantum phase transition Superfluid-to-Mott insulator in optical lattice has been shown feasible [20].

3.1.2 Local Detection in an atomic Mott insulator

In this section we will report two fundamental techniques to manipulate strongly interacting bosonic Mott insulators in optical lattice. Firstly the implementation of single-site detection, which is supported by fluorescence imaging. And finally the single-spin addressing technique. Both achievements are key pieces in the spin-entanglement generation and detection reported in [18]. These techniques are crucial both for the creation of the spin-impurity at the center of the spin chain, and for detecting the experimental observables that will be described later.

Fluorescence Imaging

We begin with a brief reminder of basic fluorescence process. Lets imagine an atom as an ideal two-level system with transition frequency ω_0 and decay rate λ . To incite the fluorescence in the atom, let us consider a classical

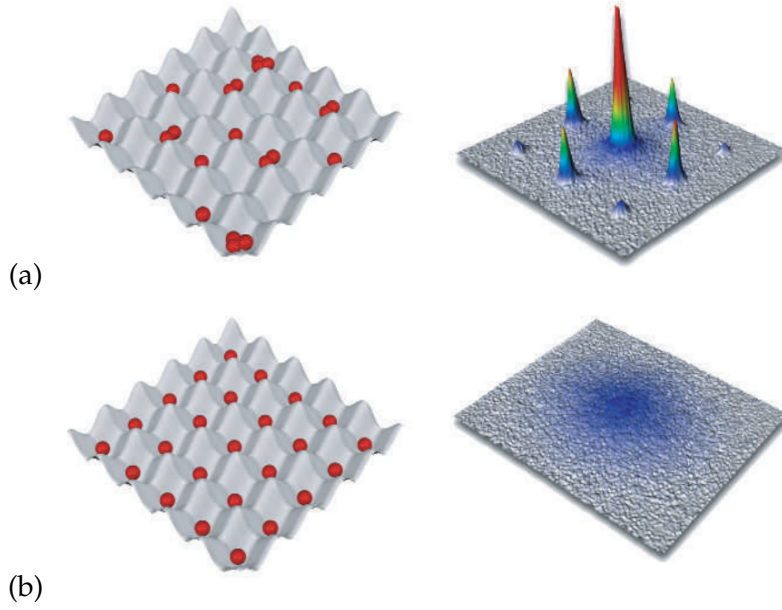


FIGURE 3.4: Superfluid-to-Mott insulator (a) Superfluid state: in the right the atoms are distributed over the sites following a Poissonian distribution and in left a matter wave interference pattern appears owing to the single-particle wave functions of the N atoms are spread out over the entire lattice (b) Mott Insulating state: in the right the lattice sites are filling with a fixed particle number, in the left the interference pattern disappears once the single-particle wave functions are confined to one site. Adapted with permission from [9].

light field

$$E(t) = E_0 \sin(\omega_L t) \quad (3.7)$$

where ω_L is the frequency of the light and E_0 is its amplitude. In this dissipative process, the photon scattering rate of an atom exposed to this light field is given by [12]

$$\Gamma_s = \frac{\lambda}{2} \left(\frac{\Omega^2/2}{\Omega^2/2\lambda^2/4 + \delta^2} \right) \quad (3.8)$$

where $\Omega = dE_0/\hbar$ is the Rabi frequency, d is the dipole matrix element of the transition and $\delta = \omega_0 - \omega_L$ is the detuning.

The fluorescence imaging is based on the spatially resolved detection of scattered photons. The main experiment that will be reported in the following sections [18], an ultracold gas of ^{87}Rb is loaded in an optical lattice. In such a frame, an optical molasses induces the fluorescence [39]. Optical molasses are a laser cooling based on Doppler cooling mechanism [1]. In this technique, an additional set of counter-propagating light waves that are superimposed over the optical lattice. Roughly speaking, this phenomenon relies on the fact that when an atom absorbs and re-emits a photon, its momentum changes. However, the important thing is that through this cooling process, the atoms isotropically emit photons with a scattering rate (3.8). So during an exposure period of optical molasses, a high-resolution microscope can collect the photons performing the fluorescence imaging. A schematic illustration of the experimental setup is given in Figure 3.5.

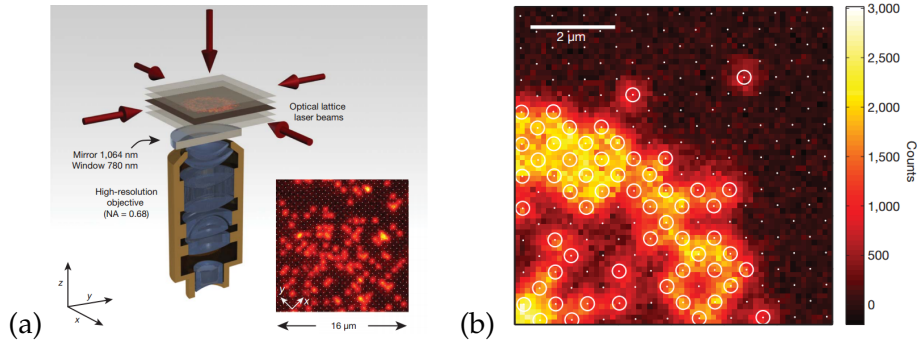


FIGURE 3.5: Fluorescence imaging of an atomic Mott insulator. (a) Experimental set-up. (b) By imaging processing an algorithm [39] determine the centers of the lattice (white points). .Adopted with permission from [39]

Single-Spin Addressing

Here we will show how the addressing of a single spin is performed at specific site of an optical lattice (see full description in [46]). The addressing technique is performed using the same microscope used for fluorescence imaging. So that the already existing optical microscope is used to overlap an additional addressing beam which is focused onto the the atomic sample by the optical imaging system. Since we are dealing with ultracold gas of ^{87}Rb , a pseudo-spin $1/2$ is encoded in two convenient hyperfine states: $|1\rangle \equiv |F = 1, m_F = -1\rangle$ and $|0\rangle \equiv |F = 2, m_F = -2\rangle$. So the addressing beam causes a localized light shift of the two hyperfine levels that tunes the addressed atom into resonance with an external microwave field. Thus allowing the coherent local spin flip of atoms in the lattice (see Figure 3.6).

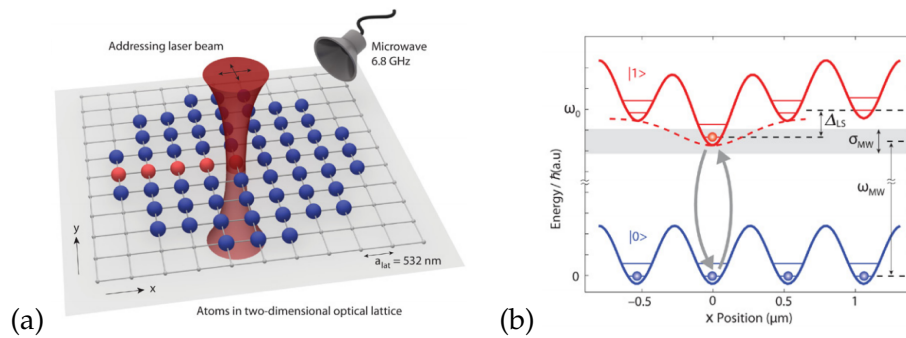


FIGURE 3.6: Addressing scheme. (a) schematic illustration of addressing technique in an atomic Mott insulator with unity filling on a 2D lattice. (b) Energy diagram of atoms with two energy states $|0\rangle$ and $|1\rangle$, the addressing beam induces resonance with external microwave field by a localized shift on state $|1\rangle$ that bring the atom from $|0\rangle$ to $|1\rangle$.

Adapted with permission from [46]

As mentioned, this technique plays an important role in the experimental setup of [18]. In which is used to create the spin-impurity at the center of the spin chains performed in the experiment [18].

3.1.3 Entanglement during spin-impurity dynamics

In this section we will describe the entanglement during spin-impurity dynamics in the spin-1/2 XX -chain [41, 2]. This approach will be useful to give theoretical predictions that support the experimental procedure [18] to be described in the next section.

Deep in the Mott-insulator regime with unity filling, a Bose-Hubbard system described by (3.6) can be mapped to the isotropic spin-1/2 Heisenberg Hamiltonian [13]:

$$\begin{aligned}\hat{H} &= -J_{ex} \sum_j \hat{\mathbf{S}}_j \cdot \hat{\mathbf{S}}_{j+1} \\ &= -J_{ex} \sum_j (\hat{S}_j^+ \hat{S}_{j+1}^- + \hat{S}_j^- \hat{S}_{j+1}^+) - J_{ex} \sum_j \hat{S}_j^z \hat{S}_{j+1}^z,\end{aligned}\quad (3.9)$$

where $\hat{S}_j^\pm = \hat{S}_j^x \pm i\hat{S}_j^y$ are the spin-1/2 raising (lowering) operators. J_{ex} is the exchange coupling, which has a constant value $J_{ex} = 4J^2/U$ for homogeneous chains (see the supplementary information of [17]).

In the case of a single spin-impurity in a 1D lattice (single excitation subspace), the Hamiltonian (3.9) can be simplified. The term $J_{ex} \sum_j \hat{S}_j^z \hat{S}_{j+1}^z$ can be neglected, since it gives rise only to an energy offset [17]. So

$$\hat{H}_{XX} = -J_{ex} \sum_j (\hat{S}_j^+ \hat{S}_{j+1}^- + \hat{S}_j^- \hat{S}_{j+1}^+). \quad (3.10)$$

The above Hamiltonian gives us a sufficient description of a spin-impurity dynamic in a 1D lattice.

A spin chain of size L with a single spin-up spin-impurity on site j can be represented by the state

$$|j\rangle \equiv |1_{-L/2}, \dots, 1_{j-1}, 0_j, 1_{j+1}, \dots, 1_{L/2-1}\rangle, \quad (3.11)$$

where $|1\rangle$ and $|0\rangle$ refers to spin down and spin up states respectively, in the z -basis. Choosing as initial state a single spin-up spin-impurity at the center of the chain, (3.11) becomes

$$|\psi_0\rangle = |j=0\rangle = |1_{-L/2}, \dots, 1_{-1}, 0_0, 1_{+1}, \dots, 1_{L/2-1}\rangle. \quad (3.12)$$

In this case, the spreading of this spin-impurity is given by the time evolution under (3.10), which can be described by

$$|\psi(t)\rangle = \sum_j \phi_j |j\rangle \quad (3.13)$$

where $\phi_j = i^j J_j(J_{ex}t/\hbar)$, in which $J_j(x)$ is the Bessel function of the first kind [28].

Concurrence between two sites

The next step is to quantify the entanglement between spins in two different sites in the chain. The reduced density operator related to a pair of different

arbitrary sites A and B is given by:

$$\psi_{AB}(t) = \text{tr}_{l \neq A, B} [|\psi(t)\rangle\langle\psi(t)|]. \quad (3.14)$$

Using (3.13) and the basis states $|00\rangle$, $|01\rangle$, $|10\rangle$ and $|11\rangle$ for sites A and B , we get:

$$\psi_{AB} = \begin{pmatrix} 0 & 0 & 0 & 0 \\ 0 & |\phi_A|^2 & \phi_A \phi_B^* & 0 \\ 0 & \phi_A^* \phi_B & |\phi_B|^2 & 0 \\ 0 & 0 & 0 & 1 - |\phi_A|^2 - |\phi_B|^2 \end{pmatrix}. \quad (3.15)$$

The matrix representation (3.15) of ψ_{AB} can be identified as X -matrix form

$$X = \begin{pmatrix} X_{11} & 0 & 0 & X_{14} \\ 0 & X_{22} & X_{23} & 0 \\ 0 & X_{32} & X_{33} & 0 \\ X_{41} & 0 & 0 & X_{44} \end{pmatrix}, \quad (3.16)$$

in which the concurrence $\mathcal{C}(X)$ can be easily calculated [48]:

$$\mathcal{C}(X) = 2 \max\{0, |X_{14}| - \sqrt{X_{22}X_{33}}, |X_{23}| - \sqrt{X_{11}X_{44}}\} \quad (3.17)$$

Thus, the concurrence $\mathcal{C}(\psi_{AB})$ between A and B sites is

$$\mathcal{C}(\psi_{AB}) = 2|\phi_A \phi_B^*|. \quad (3.18)$$

The Figure 3.7 illustrates the entanglement dynamics between symmetric sites with respect to the center of the spin chain.

3.1.4 Measuring a Lower Bound for Concurrence

Until this section it was reviewed the main aspects that support the realizations with ultracold atoms in optical lattices: we saw how to store, detect and manipulate neutral cold gases in optical lattices, and we drew a simple model to spin-impurity dynamics in 1D spin chain.

So now we are able to properly describe the experimental realization presented in [18]. In which, following the proposal [30], it was possible, due to the spatially resolved detection of spins, to observe entanglement waves in Hubbard systems with ultracold atoms.

Experimental Procedure

The experimentalists In the following, we describe the realization [18] in four principal steps:

- In the first step the experimentalists started with the preparation of an 2D sample of ultracold 170 ^{87}Rb atoms confined in a single antinode of a vertical standing wave in the z direction with a depth of $V_z = 20E_r$ (See Figure 3.8(a)), remember that E_r is the recoil energy related to the atomic mass of ^{87}Rb .
- Next by two counter-propagating laser beams along x and y directions arise two horizontal lattices with $V_x = V_y = 40E_r$ depth that drove atoms in the center of the sample to the Mott insulating regime with unity filling, forming a homogeneous grid 9×9 (Figure 3.8(b)).

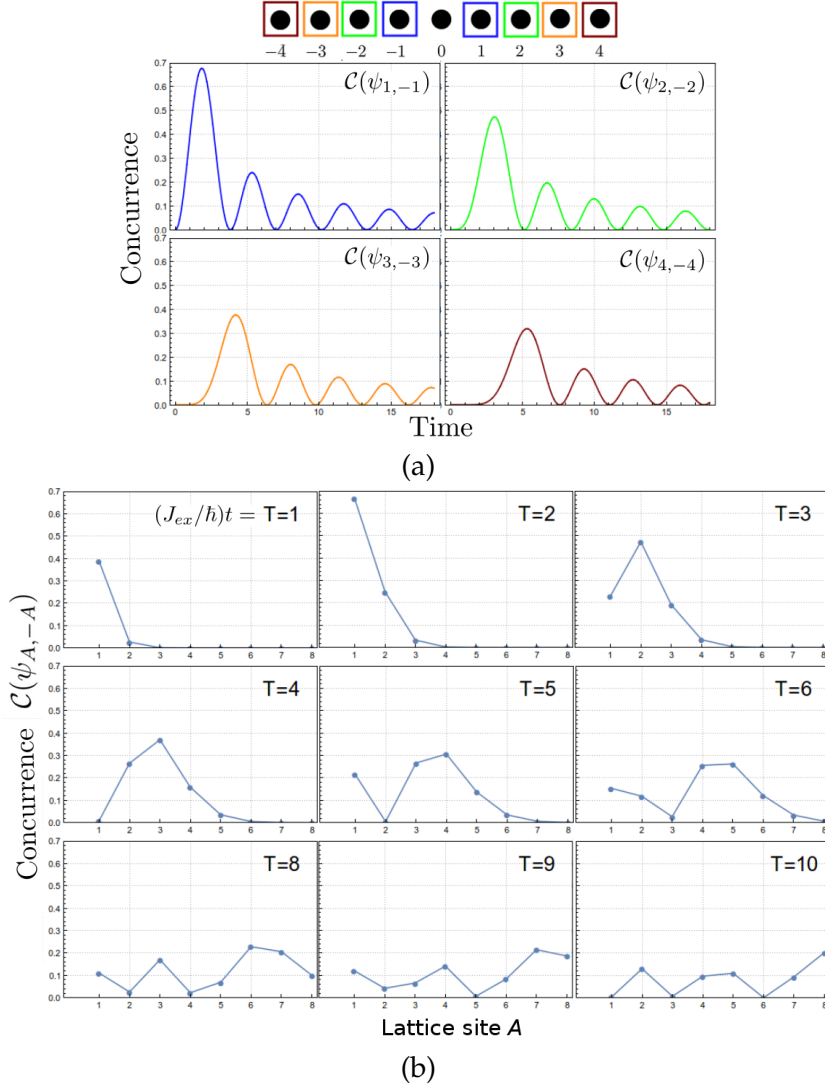


FIGURE 3.7: **Concurrence $\mathcal{C}(\psi_{A,-A})$ between sites A and $-A$ for different sites.** (a) time evolution of concurrence (b) spatial evolution of entanglement

- The system is ready to local spin flip procedure. The atoms of the center of the sample were prepared in the hyperfine state $|1\rangle \equiv |F = 1, m_F = -1\rangle$. Using single-site addressing technique, they create a spin-impurity line (in y axis) in the center of the 9×9 lattice by changing the hyperfine state of the atoms to the state $|0\rangle \equiv |F = 2, m_F = -2\rangle$. And keeping the addressing beam on, they decrease the potential depth of lattice along the x direction to $V_x = 10E_r$, forming nine parallel 1D chains of nine atoms with an spin-impurity in the center (Figure 3.8(c)).
- Finally, switching off the addressing beam, the 1D spin-impurity dynamics get started (Figure 3.8(d)). In order to stop the dynamic, the depth of all lattices are increased. The imaging of the $|0\rangle$ states was performed following two steps. Firstly, using a global microwave pulse, the entire spin population is inverted ($|0\rangle \rightarrow |1\rangle$ and $|1\rangle \rightarrow |0\rangle$).

And then, using a laser pulse resonant with the $F = 2$ to $F' = 3$ transition, the states $|0\rangle$ are pushed out of the lattice. So the site-resolved fluorescence imaging can be performed over the remaining atoms (in which relates to the atoms in the state $|1\rangle$ that, before the inversion of population $|0\rangle \rightarrow |1\rangle$, were in the state $|0\rangle$).

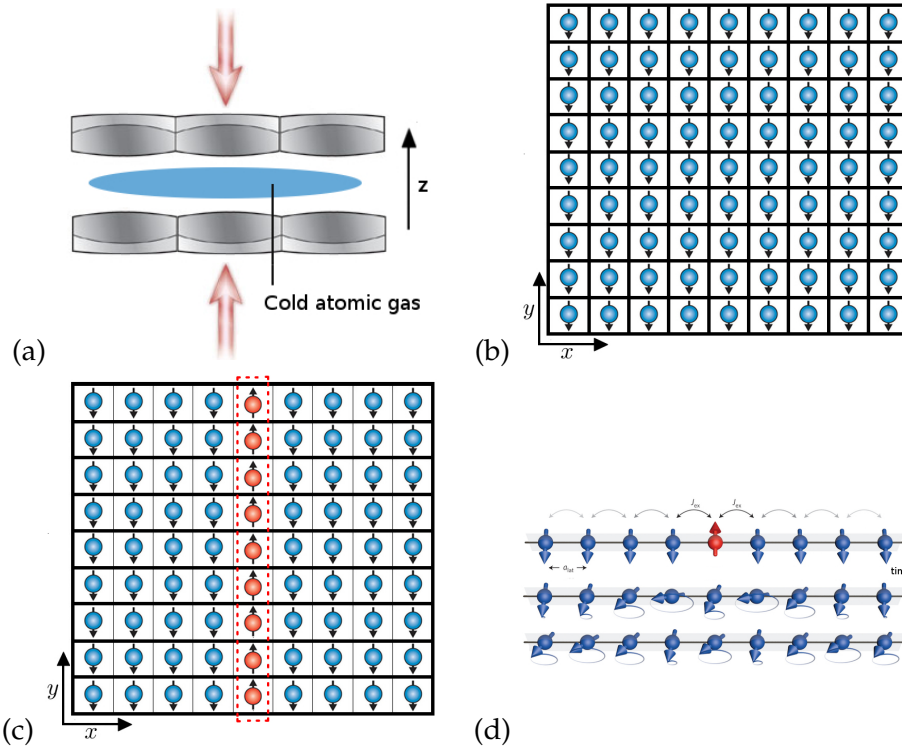


FIGURE 3.8: Experimental procedure

Two main experimental observables are measured after the experimental procedure described above. The first is the probability $P_{j\parallel}^1$ to find one atom at site j after a longitudinal (\parallel) measurement that corresponds to the probability for the atom to be in the $|1\rangle$ state. And the second, the probability $P_{j\perp}^1$ to find one atom at site j in the state $|1\rangle$ after a "transverse" measurement (\perp), in this situation we added a global $\pi/2$ rotation before the imaging of the spins.

Lower Bound for Concurrence

To measure the entanglement between two sites, the experimentalists followed the proposal [30], in which a measurable lower bound for the concurrence is derived.

Experimentally, the concurrence of an unknown state can be calculated by a full state tomography. For two spin-1/2 systems the tomography is performed by measuring fifteen combinations of Pauli matrices [36]. The elements can be detected in a measurement in the z -basis if we apply pulses that rotate the individual spins before the measurement

However, for Bose-Hubbard spin systems performed in optical lattices, the full state tomography is still a challenge. Since in this realizations individual rotations are unfeasible, only the detection of $\hat{S}_i^\alpha \hat{S}_j^\alpha$ with $\alpha =$

x, y, z by global pulses are achievable. Considering this limitation, the proposal [30] present a measurable lower bound for the concurrence using only global pulses:

$$\mathcal{K}(\psi_{ij}) = 2(2\langle \hat{S}_i^\perp \hat{S}_j^\perp \rangle - \sqrt{P_{ij}^{11} P_{ij}^{00}}) \quad (3.19)$$

where $\langle \hat{S}_i^\perp \hat{S}_j^\perp \rangle = (\langle \hat{S}_i^x \hat{S}_j^x \rangle + \langle \hat{S}_i^y \hat{S}_j^y \rangle)/2$ and P_{ij}^{11} (P_{ij}^{00}) is the joint probability of the spins on sites i and j being in the state $|1\rangle$ ($|0\rangle$). Using (3.15) in this bound equation, we find [30]

$$\begin{aligned} \mathcal{K}(\psi_{ij}) &= \mathcal{C}(\psi_{ij}), \text{ for even distances } i - j, \\ \mathcal{K}(\psi_{ij}) &= 0, \text{ for odd distances } i - j. \end{aligned} \quad (3.20)$$

So the lower bound $\mathcal{K}(\psi_{ij})$ is exactly the concurrence for spins at even distances, this result reflect the fact that in this case the spins are parallel with the $x - y$ plane, $|\langle \hat{S}_i^x \hat{S}_j^x \rangle| = |\langle \hat{S}_i^y \hat{S}_j^y \rangle| > 0$ and $|\langle \hat{S}_i^x \hat{S}_j^y \rangle| = |\langle \hat{S}_i^y \hat{S}_j^x \rangle| = 0$. On the other hand, $\mathcal{K}(\psi_{ij}) = 0$ for odd distances, in this case the spins have perpendicular alignment in the sense that $|\langle \hat{S}_i^x \hat{S}_j^x \rangle| = |\langle \hat{S}_i^y \hat{S}_j^y \rangle| = 0$ and $|\langle \hat{S}_i^x \hat{S}_j^y \rangle| = |\langle \hat{S}_i^y \hat{S}_j^x \rangle| > 0$.

Now in the experimental frame described early, we will identify the experimental observable, in which the bound (3.19) can be detected. Neglecting defects in the spin chain the operator \hat{S}_i^\perp is related to the transverse probability $P_{i\perp}^1$ by

$$P_{i\perp}^1 = \langle \hat{S}_i^\perp \rangle + \frac{1}{2}. \quad (3.21)$$

Hence

$$\langle \hat{S}_i^\perp \hat{S}_j^\perp \rangle = P_{ij\perp}^{11} - \frac{1}{4} \quad (3.22)$$

So we can rewrite (3.19) as follows

$$\mathcal{K}(\psi_{ij}) = 2(2P_{ij\perp}^{11} - \sqrt{P_{ij\parallel}^{11} P_{ij\parallel}^{00}}) - 1 \quad (3.23)$$

where $P_{ij\perp}^{11}$ is the joint probability to find one atom in the state $|1\rangle$ at site i and one at site j in the transverse measurement. Analogously, $P_{ij\parallel}^{11}$ ($P_{ij\parallel}^{00}$) is the joint probability to find one (zero) atom n site i and j in the longitudinal measurement, remembering that at the end of the experimental procedure (fourth step) before the inversion of populations ($|0\rangle \rightarrow |1\rangle$ and $|1\rangle \rightarrow |0\rangle$) only the atoms with state $|0\rangle$ remain in the lattice.

In addition to (3.23), a more efficient lower bound is derived in [18], this one non-perfect initial Mott insulator are taken into account, resulting in $P_{i\perp}^1 < 0.5$. In that case the perpendicular correlation (3.22) is given by $\langle \hat{S}_i^\perp \hat{S}_j^\perp \rangle = P_{ij\perp}^{11} - P_{i\perp}^1 P_{j\perp}^1$. Then (3.23) is rewritten as

$$\tilde{\mathcal{K}}(\psi_{ij}) = 2(2(P_{ij\perp}^{11} - P_{i\perp}^1 P_{j\perp}^1) - \sqrt{P_{ij\parallel}^{11} P_{ij\parallel}^{00}}) \quad (3.24)$$

In Figure 3.9 are shows the results for both lower bounds for the concurrence (3.23) and (3.24) for symmetric pairs around the center of the spin chain.

Since we aimed in a brief overview about experimental realization [18] some aspects was neglected. For a more detailed description of the experimental procedure it is recommend to see [18] and the references there.

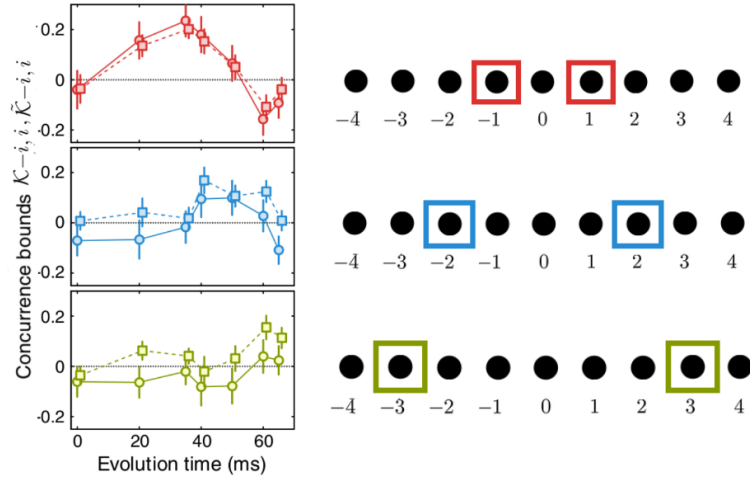


FIGURE 3.9: Propagation of entanglement. Experimental lower bound for the concurrence $\mathcal{K}_{-i,i}$ (circles with solid line) and the more efficient bound $\tilde{\mathcal{K}}_{-i,i}$ [18] (squares with dashes line). Adapted with permission from [18].

Issues such as inhomogeneity in the lattice potential, holes or multiple-occupied lattice sites and their influence on entanglement detection are well described there.

3.2 Coarse-grained Entanglement in a Spin Chain

After the description of the experimental accomplishment [18], finally we can properly present the main proposal of this chapter. As mentioned before and supported by previous sections, we verify that realizations like [18] spend high experimental resource. Especially in the single site detection, using fluorescence imaging, the need for high accurate equipments, like high-resolution microscopy, can become an impediment. In order to overcome these experimental difficulties, is desirable to devise an approach that dispenses this high precision, with the detection of entanglement remaining viable.

To describe this situation we will use the coarse-graining model proposed in the last chapter. Assuming the experimental adversity, where our microscope doesn't have enough definition to perform single site detection, in this section we will propose a suitable coarse graining map to simulate this blurred detection in order to study the loss of entanglement information.

We start with the simple case, to simulate a blurred detector lets consider the experimental situation: We wish measure the spin information from two neighboring atoms, but in the fluorescence imaging our detector doesn't have enough resolution to resolve the light coming from each single site in the lattice. Furthermore we consider that the amount of light in the fluorescence of a single atom is sufficient to saturate the detector.

Thus, in this scenario, states like $|01\rangle$, $|10\rangle$ and $|11\rangle$, yield the same signal, hence we can not distinguish them. Motivated by such situations, this loss of information can be described by a coarse graining map Λ_{CG} :

$\mathcal{L}(\mathcal{H}_4) \rightarrow \mathcal{L}(\mathcal{H}_2)$:

$$\begin{aligned}
\Lambda_{CG}(|00\rangle\langle 00|) &= |0\rangle\langle 0| & \Lambda_{CG}(|10\rangle\langle 00|) &= \frac{1}{\sqrt{3}}|1\rangle\langle 0| \\
\Lambda_{CG}(|00\rangle\langle 01|) &= \frac{1}{\sqrt{3}}|0\rangle\langle 1| & \Lambda_{CG}(|10\rangle\langle 01|) &= 0 \\
\Lambda_{CG}(|00\rangle\langle 10|) &= \frac{1}{\sqrt{3}}|0\rangle\langle 1| & \Lambda_{CG}(|10\rangle\langle 10|) &= |1\rangle\langle 1| \\
\Lambda_{CG}(|00\rangle\langle 11|) &= \frac{1}{\sqrt{3}}|0\rangle\langle 1| & \Lambda_{CG}(|10\rangle\langle 11|) &= 0 \\
\Lambda_{CG}(|01\rangle\langle 00|) &= \frac{1}{\sqrt{3}}|1\rangle\langle 0| & \Lambda_{CG}(|11\rangle\langle 00|) &= \frac{1}{\sqrt{3}}|1\rangle\langle 0| \\
\Lambda_{CG}(|01\rangle\langle 01|) &= |1\rangle\langle 1| & \Lambda_{CG}(|11\rangle\langle 01|) &= 0 \\
\Lambda_{CG}(|01\rangle\langle 10|) &= 0 & \Lambda_{CG}(|11\rangle\langle 10|) &= 0 \\
\Lambda_{CG}(|01\rangle\langle 11|) &= 0 & \Lambda_{CG}(|11\rangle\langle 11|) &= |1\rangle\langle 1|.
\end{aligned} \tag{3.25}$$

In the above coarse graining map the factor $1/\sqrt{3}$ ensures the trace preserving and completely positiveness of the operation. And since we cannot distinguish the states $|01\rangle$, $|10\rangle$ and $|11\rangle$, there can be no coherence in this subspace, so the above null terms appear.

3.2.1 Coarse-Grained Entanglement Dynamics

Once we have already constructed our coarse graining map (3.25) that plays the role of a blurred detector, lets study how the entanglement evolves under this coarse graining view. In the same way as detection performed in [18], we will calculate the entanglement behavior between two symmetric sites around the center of a coarse-grained chain. We will take two different degrees of resolution: first we map two sites as an effective one, and then four sites as a single one. So that, this approach enables us to study how this coarse graining process affects the entanglement in the chain, giving us the possibility to qualitatively argue for an experimental boundary in which the experimental detection of entanglement is still possible.

Firstly we need to characterize the state that through our blurred detector we don't have complete access. To compute the first coarse graining level where two sites will be mapped to a single one, we represent the state in reduced density operator formalism of two arbitrary pairs of two neighboring sites in the lattice (A_1 - A_2 and B_1 - B_2):

$$\psi' = \text{tr}_{l \neq A_1, A_2, B_1, B_2} [|\psi(t)\rangle\langle\psi(t)|], \tag{3.26}$$

since $|\psi(t)\rangle$ is given by (3.13)

$$\begin{aligned}
\psi' &= |\phi_{A_1}|^2 |10\rangle\langle 10| \otimes |00\rangle\langle 00| + \phi_{A_1} \phi_{A_2}^* |10\rangle\langle 01| \otimes |00\rangle\langle 00| + \\
&+ \phi_{A_1} \phi_{B_1}^* |10\rangle\langle 00| \otimes |00\rangle\langle 10| + \phi_{A_1} \phi_{B_2}^* |10\rangle\langle 00| \otimes |00\rangle\langle 01| + \\
&+ \phi_{A_2} \phi_{A_1}^* |01\rangle\langle 10| \otimes |00\rangle\langle 00| + |\phi_{A_2}|^2 |01\rangle\langle 01| \otimes |00\rangle\langle 00| + \\
&+ \phi_{A_2} \phi_{B_1}^* |01\rangle\langle 00| \otimes |00\rangle\langle 10| + \phi_{A_2} \phi_{B_2}^* |01\rangle\langle 00| \otimes |00\rangle\langle 01| + \\
&+ \phi_{B_1} \phi_{A_1}^* |00\rangle\langle 10| \otimes |10\rangle\langle 00| + \phi_{B_1} \phi_{A_2}^* |00\rangle\langle 01| \otimes |10\rangle\langle 00| + \\
&+ |\phi_{B_1}|^2 |00\rangle\langle 00| \otimes |10\rangle\langle 10| + \phi_{B_1} \phi_{B_2}^* |00\rangle\langle 00| \otimes |10\rangle\langle 01| + \\
&+ \phi_{B_2} \phi_{A_1}^* |00\rangle\langle 10| \otimes |01\rangle\langle 00| + \phi_{B_2} \phi_{A_2}^* |00\rangle\langle 01| \otimes |01\rangle\langle 00| + \\
&+ \phi_{B_2} \phi_{B_1}^* |00\rangle\langle 00| \otimes |01\rangle\langle 10| + |\phi_{B_2}|^2 |00\rangle\langle 00| \otimes |01\rangle\langle 01| + \\
&+ (1 - |\phi_{A_1}|^2 + |\phi_{A_2}|^2 + |\phi_{B_1}|^2 + |\phi_{B_2}|^2) |00\rangle\langle 00| \otimes |00\rangle\langle 00|
\end{aligned} \tag{3.27}$$

then applying the map defined by (3.25), we can easily calculate the coarse-grained state:

$$\begin{aligned} \psi^{CG} &= (\Lambda_{CG} \otimes \Lambda_{CG})(\psi') \\ &= \begin{pmatrix} \zeta & 0 & 0 & 0 \\ 0 & |\phi_{B_1}|^2 + |\phi_{B_2}|^2 & \frac{1}{3}(\phi_{A_1} + \phi_{A_2})^*(\phi_{B_1} + \phi_{B_2}) & 0 \\ 0 & \frac{1}{3}(\phi_{A_1} + \phi_{A_2})(\phi_{B_1} + \phi_{B_2})^* & |\phi_{A_1}|^2 + |\phi_{A_2}|^2 & 0 \\ 0 & 0 & 0 & 0 \end{pmatrix}, \end{aligned} \quad (3.28)$$

where $\zeta = 1 - |\phi_{A_1}|^2 - |\phi_{A_2}|^2 - |\phi_{B_1}|^2 - |\phi_{B_2}|^2$, and ψ_{CG} is expressed using the basis states $|00\rangle$, $|01\rangle$, $|10\rangle$ and $|11\rangle$ for the resulting two coarse-grained sites.

For the next level of resolution, where we want map four sites as a single one, we compute the reduced state to an arbitrary pair of four neighboring atoms (A_1 - A_2 - A_3 - A_4 and B_1 - B_2 - B_3 - B_4):

$$\psi' = \text{tr}_{l \neq A_1, A_2, A_3, A_4, B_1, B_2, B_3, B_4} |\psi(t)\rangle\langle\psi(t)|. \quad (3.29)$$

To calculate the coarse-grained state in this second coarse graining level we compose the map (3.25) and apply over (3.29):

$$\psi^{CG} = (\Lambda_{CG} \circ (\Lambda_{CG} \otimes \Lambda_{CG})) \otimes (\Lambda_{CG} \circ (\Lambda_{CG} \otimes \Lambda_{CG}))(\psi'). \quad (3.30)$$

Once characterized the coarse-grained states, let us calculate their concurrences.

Concurrence

To detect the entanglement between two coarse-grained sites we will derive an equation for the concurrence analogous to that found before for two (non-coarse-grained) sites in (3.18).

To calculate the concurrence in the first coarse graining level, where we map two sites as one, we use the result (3.17), since ψ^{CG} in (3.28) takes the X -matrix form. Then the concurrence is given by

$$\mathcal{C}(\psi^{CG}) = \frac{2}{3} |(\phi_{A_1} + \phi_{A_2})(\phi_{B_1} + \phi_{B_2})^*|. \quad (3.31)$$

At first sight this equation looks like the form of concurrence between two sites in (3.18).

For the purpose of giving a concrete view about the consequences of result (3.31), we will study the entanglement evolution in a chain with seventeen sites in the "microscopic" level. We will plot the concurrence between the symmetric sites around the center of the chain, and compare with their respective coarse-grained site. In this first coarse graining level we use the equation (3.18) to calculate the concurrence between the first two pair of sites before the coarse graining: $\mathcal{C}(\psi_{1-1}) = 2|\phi_1\phi_{-1}^*|$ and $\mathcal{C}(\psi_{2-2}) = 2|\phi_2\phi_{-2}^*|$. Then, we calculate the concurrence of the resulting pair of coarse-grained sites using the equation (3.31): $\mathcal{C}(\psi_{1,-1}^{CG}) = (2/3)|(\phi_1 + \phi_2)(\phi_{-1} + \phi_{-2})^*|$.

$\phi_{-2})^*$. In the same way we calculate the concurrence between others symmetric sites around the center both at the "microscopic" level and at coarse-grained level. The results are shown in Figure 3.10.

From this first coarse graining level we find some interesting results. In Figure 3.10(a), we observe that the concurrence decay in the coarse graining level. Despite of this, a significant amount of entanglement still survives. So even in the coarse graining description we observe an outwards propagating entanglement "wave" (See 3.10(b) and 3.10(c)). In this scenario, we can speculate that in a realistic experimental procedure the entanglement would still be detectable.

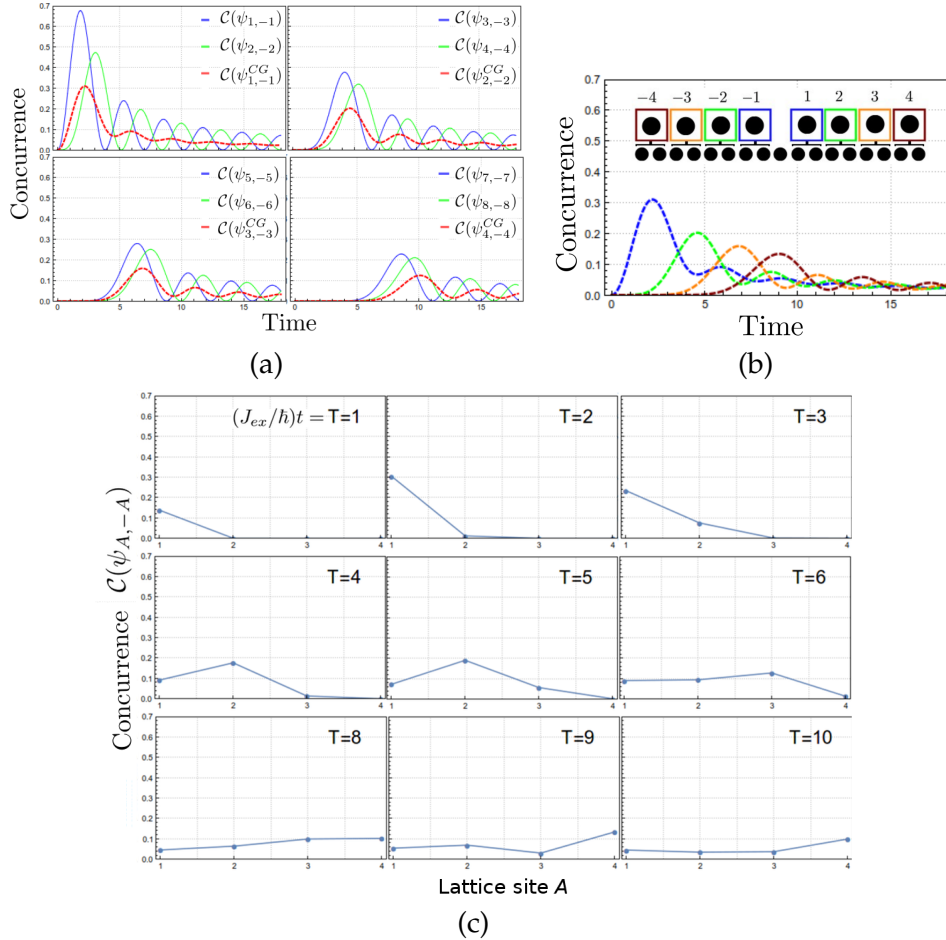


FIGURE 3.10: Concurrence $\mathcal{C}(\psi_{A,-A})$. (a) Here we show the concurrence evolution between the first eight symmetric pairs of sites in the spin chain, $\mathcal{C}(\psi_{A,-A})$, and the concurrence between the resulting coarse-grained sites. (b) Time evolution of concurrence $\mathcal{C}(\psi_{A_{CG},-A_{CG}}^{CG})$ in the CG level (c) spatial dynamics of concurrence in the CG level.

For the next coarse graining level, in which four sites in the lattice are mapped to one, we proceed in an analogous way. From (3.30) using the result of concurrence of X states (3.17), we have:

$$\mathcal{C}(\psi^{CG}) = \frac{2}{9} |(\phi_{A_1} + \phi_{A_2} + \phi_{A_3} + \phi_{A_4})(\phi_{B_1} + \phi_{B_2} + \phi_{B_3} + \phi_{B_4})^*|. \quad (3.32)$$

Note that this result preserves the same structure as the (3.31). To see how

the concurrence behave in this coarse graining level we consider again a chain composed of seventeen sites with the spin-impurity starting in the center. Since we will calculate the concurrence between pair of sites symmetric to the center we note that in this coarse graining level we have only two pairs of coarse-grained sites (since the chain is composed of seventeen sites) where each coarse-grained site comes from the blurred detection of four sites in the "microscopic" level.

Considering again a chain with seventeen sites lets see how the entanglement evolves in this coarse-grained level. Analogously with the last case, we plot the concurrence between the symmetric sites around the center of the chain, and compare it with their respective coarse-grained sites. We use the equation (3.18) to calculate the concurrence between the first four pair of sites before the coarse graining: $\mathcal{C}(\psi_{1-1}) = 2|\phi_1\phi_{-1}^*|$, $\mathcal{C}(\psi_{2-2}) = 2|\phi_2\phi_{-2}^*|$, $\mathcal{C}(\psi_{2-3}) = 2|\phi_2\phi_{-3}^*|$ and $\mathcal{C}(\psi_{4-4}) = 2|\phi_4\phi_{-4}^*|$. Then, we calculate the concurrence of the resulting pair of coarse-grained sites using the equation (3.32): $\mathcal{C}(\psi^{CG}) = \frac{2}{9}|(\phi_1 + \phi_2 + \phi_3 + \phi_4)(\phi_{-1} + \phi_{-2} + \phi_{-3} + \phi_{-4})^*|$. We proceed in the same way to calculate the concurrence between the other symmetric sites. See the results in the Figure 3.11.

Now let us analyze the results in this second resolution level, where we have mapped four sites to one. In 3.11(a), as expected, we observe that the concurrence becomes weak compared to the concurrence in the "microscopic" level or in the first coarse graining level (saw in 3.10). Consequently we observe an weak outwards propagating entanglement "wave", now confined to only two coarse graining sites (see 3.10(b) and 3.10(c)). Therefore in this scheme, we guess that in a realistic experimental procedure the entanglement would no longer be detectable.

Negativity

Another way of studying the differences in the entanglement between the "microscopic" level and the coarse graining level is through negativity \mathcal{N} . Using concurrence we are restrict to calculate only entanglement between two qubits (two sites in the spin-chain). With the negativity we can explore another possibilities, as we can calculate the entanglement between qudits. What means that we can calculate entanglement between two or more spins in the chain, no more restricted to pair of spins.

Instead of studying many situations as we did for concurrence, here we will limit ourselves to study the negativity in a single simple case. Considering an spin-chain composed of five spins (see Figure 3.12) we calculate the negativity between sites 1 and 2 with respect to their symmetrical sites (-1 and -2). This can be easily calculated using the equation (2.53) for negativity defined in last chapter, and the reduced state (3.27) that describes this situation. For the related coarse graining level, we calculate the negativity using (3.28) in (2.53). Results are shown in Figure (3.12). Beyond the decay of entanglement also observed using the concurrence as measure of entanglement, with negativity we can observe that the instant where the maximum value of negativity is reached both for the "microscopic" level and for the coarse-grained level it seems to be the same, this is an interesting result.

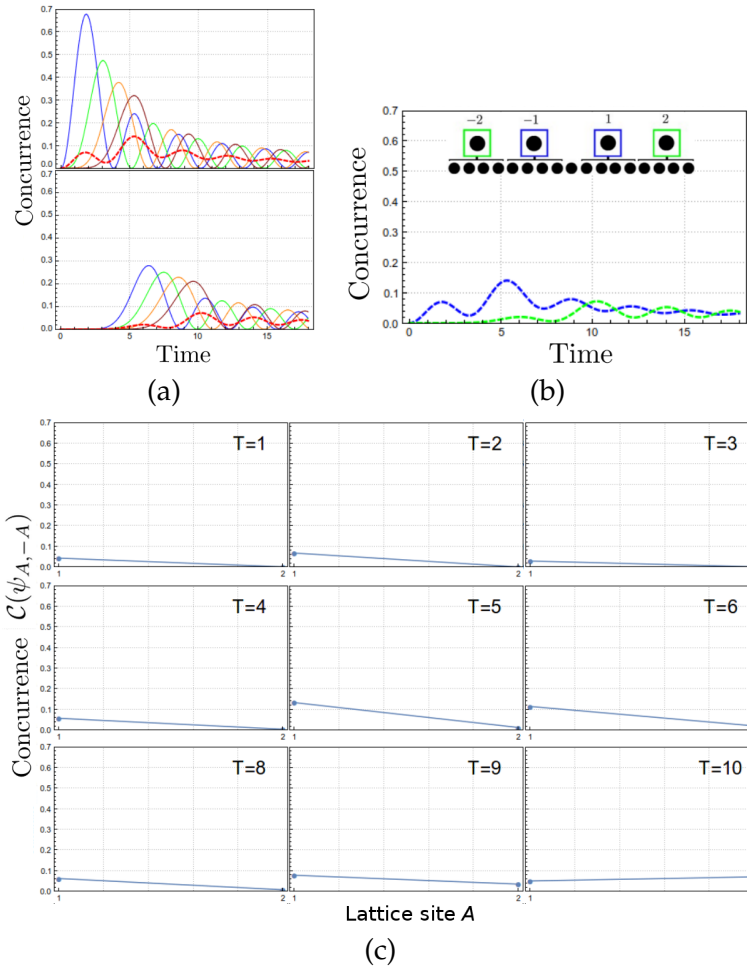


FIGURE 3.11: Concurrency $\mathcal{C}(\psi_{A,-A})$. (a) Here we show the concurrency evolution between the first eight symmetric pairs of sites in the spin chain, $\mathcal{C}(\psi_{A,-A})$, and the concurrency between the resulting coarse-grained sites. (b) Time evolution of concurrency in the CG level (c) spatial dynamics of concurrency in the CG level.

So we end this chapter by giving a brief summary of what we have learned. Firstly we saw a theoretical model that describes the entanglement dynamics in a Heisenberg spin-chain due to the dynamics of a spin-impurity. Then we described an experimental realization using ultracold atoms in an optical lattice that accomplishes this entanglement detection in spin-chains. And finally we constructed a coarse graining map that models an experimental procedure without full resolution in the detection of the spin-chain. As expected, since the description of the spin entangled system is taken in a smaller dimensional space, it was verified a loss of entanglement. Despite the amount of entanglement decay both for concurrency and for negativity, a considerable amount of entanglement still survives, mainly in the first coarse graining level. Thus this result indicates that in an experimental procedure with lower precision, with respect to the resolution of detection than [18], the entanglement possibly will still be detected.

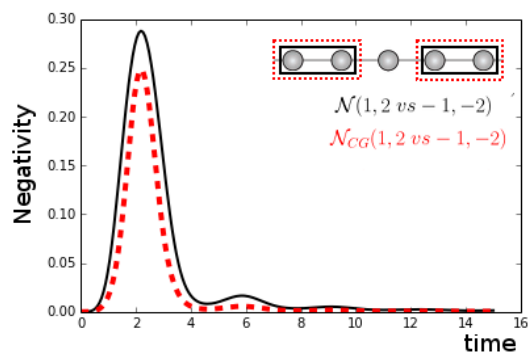


FIGURE 3.12: Negativity between the first symmetric pair of sites in the chain both at microscopic and coarse-grained levels, $\mathcal{N}(\psi_{1,2vs-1,-2})$ and $\mathcal{N}(\psi^{CG})$ respectively.

Chapter 4

Equation for Entanglement in Coarse-grained Systems

4.1 Evolution Equation for Quantum Entanglement

In realistic situations, quantum systems can not be completely isolated from their environment. In an experimental framework, for example, the interaction between the laboratory apparatus and the quantum system leads to a degradation of quantum characteristics. That is, the interaction between a quantum system and a large system (like a macroscopic object) with uncontrollable degrees of freedom leads to a decay process of the quantum features. Thus, in this decoherence dynamics, entanglement is also led to vanish.

Describing this entanglement decoherence process, especially in large quantum systems, is a challenging task. The conventional way of dealing with this problem is to follow the evolution of the system until the desired instant, perform the full state tomography, and from the result calculate its entanglement. However, for large systems tomography becomes difficult. Firstly because the manipulation techniques of some physical systems are not good enough as to measure the observables that are required for the state tomography process. Secondly, even if the tomography can be performed, the number of necessary observables to be measured grows exponentially with the number of system components, making the full state tomography at least an exhausting task. In this context, it is of fundamental interest to find an equation of motion that directly describes the dynamics of entanglement under a decoherence process.

Using the minimal information about the initial state and its dynamic process, recent works accomplished this kind of description of entanglement evolution. In [43, 29, 44], it was derived an equation for concurrence dynamics where one of the subsystems of an initial 2×2 pure state undergoes a noisy channel. By rewriting the initial state in a suitable form, the researchers have obtained a factorized equation for the concurrence. The derived equation is composed by only two independent terms: one relates to the entanglement of the initial state and the other encodes the channel parameters (this approach will be better clarified in the course of this section).

Here we will look for an analogous equation relation for $2 \times D$ initial pure states when the D -dimensional part passes through a channel. Based on the method used in [44] for 2×2 case, we will try to develop an analogous deterministic equation for concurrence, which contains only a single quantity that, independently of the initial state, describes the entanglement

evolution of the system. Of course we hope that this approach must converge to the 2×2 case when we take $D = 2$. Afterwards, using this derived equation we consider the coarse-graining operation as the channel in the equation. Doing this, the system $2 \times D$ can illustrate the measurement process, where a macroscopic detector interacts with a qubit.

4.1.1 Entanglement Under Filtering Operations

As prerequisite for what follows, let us see how states of $2 \times D$ dimensions vary under filtering operations. Here we call a filtering operation B as a quantum operation that is non-tracing-preserving $B^\dagger B \leq \mathbb{1}$. Considering an arbitrary $2 \times D$ state

$$|\psi\rangle = \sum_{i=0}^1 \sum_{j=0}^{d-1} a_{ij} |i\rangle |j\rangle \quad (4.1)$$

that suffers the action of a filtering operation $B = \sum_{k,l=0}^1 b_{kl} |k\rangle \langle l|$ on its first subsystem, the resulting normalized state is

$$|\psi'\rangle = \frac{B \otimes \mathbb{1} |\psi\rangle}{\|B \otimes \mathbb{1} |\psi\rangle\|}. \quad (4.2)$$

To calculate its concurrence, we will employ some particularities of $2 \times D$ systems. States like (4.1) have at most two non-zero Schmidt coefficients λ_i , and in Schmidt representation the reduced density operator of the first subsystem is given by $\psi'_A = \lambda_0 |0_s\rangle \langle 0_s| + \lambda_1 |1_s\rangle \langle 1_s|$, with $\{|0_s\rangle, |1_s\rangle\}$ Schmidt basis vectors. Taking these features, the equation of concurrence given by (2.49) can be rearranged as

$$\mathcal{C}(|\psi'\rangle) = 2\sqrt{\lambda_0 \lambda_1} = 2\sqrt{\det \psi'_A}. \quad (4.3)$$

From (4.2), calculating the reduced matrix ψ'_A

$$\begin{aligned} \psi'_A &= \text{tr}_B |\psi'\rangle \langle \psi'| \\ &= \frac{1}{\|B \otimes \mathbb{1} |\psi\rangle\|^2} \text{tr}_B (B \otimes \mathbb{1} |\psi\rangle \langle \psi| B^\dagger \otimes \mathbb{1}) \\ &= \frac{B \psi_A B^\dagger}{\|B \otimes \mathbb{1} |\psi\rangle\|^2} \end{aligned} \quad (4.4)$$

where tr_B is the partial trace over the second subsystem and $\psi_A = \text{tr}_B |\psi\rangle \langle \psi|$. So that applying (4.3), the concurrence of $|\psi'\rangle$ is given by

$$\begin{aligned} \mathcal{C}(|\psi'\rangle) &= 2\sqrt{\det \psi'_A} \\ &= 2\sqrt{\det \left(\frac{B \psi_A B^\dagger}{\|B \otimes \mathbb{1} |\psi\rangle\|^2} \right)} \\ &= \frac{|\det B|}{\|B \otimes \mathbb{1} |\psi\rangle\|^2} 2\sqrt{\det \psi_A} \\ &= \frac{|\det B|}{\|B \otimes \mathbb{1} |\psi\rangle\|^2} \mathcal{C}(|\psi\rangle), \end{aligned} \quad (4.5)$$

in the third line we used the properties: $\det(AB) = \det A \det B$, $\det B = \det B^\dagger$ and $\det(aB) = a^n \det B$ for an $n \times n$ matrix. Thus filtering operations redefine the concurrence by $\det B$. So by an appropriate combination of filtering operations, entanglement can be increased or decreased.

We can extend this approach to mixed states. A filtered mixed state is

$$\psi' = \frac{(B \otimes \mathbb{1})\psi(B^\dagger \otimes \mathbb{1})}{\text{tr}((B \otimes \mathbb{1})\psi(B^\dagger \otimes \mathbb{1}))} = \frac{\mathcal{B} \otimes \mathbb{1}(\psi)}{\text{tr}(\mathcal{B} \otimes \mathbb{1}(\psi))} \quad (4.6)$$

where \mathcal{B} is an abbreviate way to represent the action of B onto ψ . Since a mixed state can be written as $\psi = \sum_i p_i |\psi_i\rangle\langle\psi_i|$, the filtered state ψ' becomes

$$\begin{aligned} \psi' &= \frac{\mathcal{B} \otimes \mathbb{1}(\sum_i p_i |\psi_i\rangle\langle\psi_i|)}{\text{tr}(\mathcal{B} \otimes \mathbb{1}(\psi))} \\ &= \frac{1}{\text{tr}(\mathcal{B} \otimes \mathbb{1}(\psi))} \sum_i p_i \mathcal{B} \otimes \mathbb{1}(|\psi_i\rangle\langle\psi_i|) \\ &= \frac{1}{\text{tr}(\mathcal{B} \otimes \mathbb{1}(\psi))} \sum_i p_i |\psi'_i\rangle\langle\psi'_i| \end{aligned} \quad (4.7)$$

where $|\psi'_i\rangle = \mathcal{B} \otimes \mathbb{1}|\psi_i\rangle$. Considering that B is invertible, we can also relate any decomposition of ψ into state vectors $|\psi'_i\rangle$ by $|\psi_i\rangle = B^{-1} \otimes \mathbb{1}|\psi'_i\rangle$. This implies that the ensembles of pure states $\{|\psi_i\rangle\}$ and $\{|\psi'_i\rangle\}$ of the decompositions of ψ and ψ' are related only by the filtering operation. Therefore, considering the concurrence given by (2.50), if the infimum optimal decomposition of ψ is given by $\{|\psi_i\rangle\}$ with probabilities p_i , then the optimal decomposition of ψ' is realized by the same probabilities p_i with ensemble $\{|\psi'_i\rangle\}$ which are the filtered form of $\{|\psi_i\rangle\}$:

$$\begin{aligned} \mathcal{C}(\psi') &= \frac{1}{\text{tr}(\mathcal{B} \otimes \mathbb{1}(\psi))} \inf_{\{p_i, |\psi'_i\rangle\}} \sum_i p_i \mathcal{C}(|\psi'_i\rangle) \\ &= \frac{1}{\text{tr}(\mathcal{B} \otimes \mathbb{1}(\psi))} \inf_{\{p_i, |\psi_i\rangle\}} \sum_i p_i \mathcal{C}(\mathcal{B} \otimes \mathbb{1}(|\psi_i\rangle)) \end{aligned} \quad (4.8)$$

Thus, from (4.5), the concurrence of mixed states under filtering operation is given by

$$\begin{aligned} \mathcal{C}(\psi') &= \frac{|\det B|}{\text{tr}(\mathcal{B} \otimes \mathbb{1}(\psi))} \inf_{\{p_i, |\psi_i\rangle\}} \sum_i p_i \mathcal{C}(|\psi_i\rangle) \\ &= \frac{|\det B|}{\text{tr}(\mathcal{B} \otimes \mathbb{1}(\psi))} \mathcal{C}(\psi) \end{aligned} \quad (4.9)$$

4.1.2 Evolution Equation for concurrence of $2 \times D$ systems

A general quantum evolution is described by the action of a dynamical completely positive map Λ onto an initial state ψ :

$$\psi' = \Lambda(\psi). \quad (4.10)$$

For an initial bipartite state ψ the action of a dynamical map Λ over the second subsystem is described by

$$\psi' = \mathbb{1} \otimes \Lambda(\psi). \quad (4.11)$$

Such situation, for example, describes the following laboratory realization. Imagine an experimental situation in which a system with two entangled photons is prepared and subsequently one of them is sent to a distant lab through an optical fiber. It is to be expected that the transmitted photon will suffer the action of its environment (that can be mapped by a noisy channel Λ), whereas the another photon remains protected in the lab.

Considering as starting point the evolution process (4.11), we aim to develop a relation between the concurrence of the initial state $\mathcal{C}(\psi)$ and the concurrence of the final state $\mathcal{C}(\psi')$ in terms of the channel Λ (See Figure 4.1). This relation is known for 2×2 systems, from [42, 29, 44]. In this chapter we wish to extend this result to $2 \times D$, trying to keep the factorized form, which the equation for entanglement evolution is independent of the initial state, relating only to the evolution channel Λ parameters.

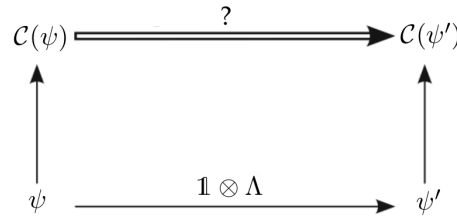


FIGURE 4.1: From a state evolution $\mathbb{1} \otimes \Lambda$, we want to find an entanglement dynamics relation between the concurrence of the initial state $\mathcal{C}(\psi)$ and the concurrence of the final state $\mathcal{C}(\psi')$

In order to derive such an evolution equation, we rewrite the equation (4.11) following some specific operations.

As first step, taking as initial $2 \times D$ state the pure state (4.1), it is convenient for what follows to express it in Schmidt representation, using (2.31):

$$|\psi\rangle = U \otimes V^* |\psi_s\rangle, \quad (4.12)$$

where $|\psi_s\rangle = \sum_k \sqrt{\lambda_k} |k\rangle |k\rangle$ and U and V are the unitary Schmidt operators. In terms of density matrix

$$\psi = \mathcal{U} \otimes \mathcal{V}^*(\psi_s), \quad (4.13)$$

where \mathcal{U} and \mathcal{V} are the simplified notation for the action of the operators U and V over density operator $\psi_s = |\psi_s\rangle\langle\psi_s|$.

So that using (4.13) in (4.11)

$$\psi' = \mathbb{1} \otimes \Lambda \circ \mathcal{U} \otimes \mathcal{V}^*(\psi_s). \quad (4.14)$$

Next, we express the Schmidt state ψ_s as the result of a local filtering operation $B = \sqrt{2} \sum_{k=0}^1 \sqrt{\lambda_k} |k\rangle\langle k|$ over the first subsystem of a maximally

entangled state $|\phi^+\rangle = (|0\rangle|0\rangle + |1\rangle|1\rangle)/\sqrt{2}$:

$$|\psi_s\rangle = B \otimes \mathbb{1}|\phi^+\rangle. \quad (4.15)$$

Defining $\phi^+ \equiv |\phi^+\rangle\langle\phi^+|$

$$\begin{aligned} \psi_s &= (B \otimes \mathbb{1})|\phi^+\rangle\langle\phi^+|(B \otimes \mathbb{1})^\dagger \\ &= \mathcal{B} \otimes \mathbb{1}(\phi^+). \end{aligned} \quad (4.16)$$

Thus we can rewrite (4.14) as follows

$$\begin{aligned} \psi' &= \mathbb{1} \otimes \Lambda \circ \mathcal{U} \otimes \mathcal{V}^* \circ \mathcal{B} \otimes \mathbb{1}(\phi^+) \\ &= \mathcal{U} \otimes \mathbb{1} \circ \mathcal{B} \otimes \mathbb{1} \circ \mathbb{1} \otimes \Lambda \mathcal{V}^*(\phi^+) \\ &= \mathcal{U} \otimes \mathbb{1} \circ \mathcal{B} \otimes \mathbb{1}(\psi_{\Lambda\mathcal{V}}), \end{aligned} \quad (4.17)$$

where $\psi_{\Lambda\mathcal{V}} \equiv \mathbb{1} \otimes \Lambda \mathcal{V}^*(\phi^+)$ is in general a mixed state such that it encodes the dynamic channel Λ and the parameters of the initial state by Schmidt operator \mathcal{V} . The operation \mathcal{B} encodes only the parameters of the initial state ψ . The choice of the maximally entangled state is irrelevant for our purpose to measure entanglement. Since $|\phi^+\rangle$ can be mapped to another maximally entangled state by act of a local unitary operation on the first qubit, $\psi_{\Lambda\mathcal{V}}$ changes but, as we have seen, the entanglement is invariant under local unitary transformations.

A schematic representation of the rescale from (4.11) to (4.17) is illustrated in the Figure 4.2

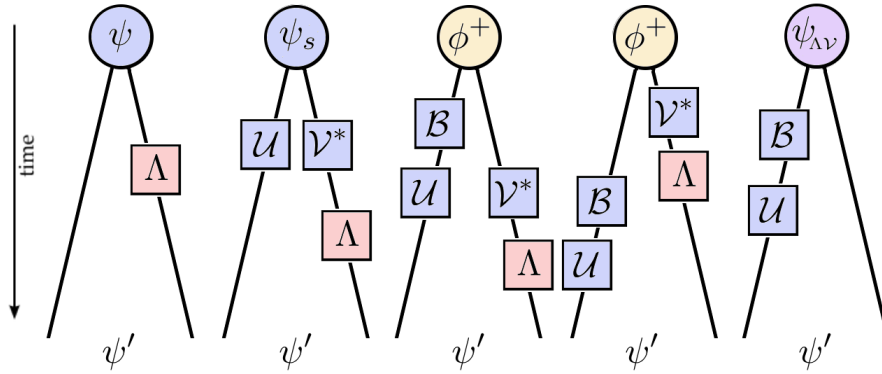


FIGURE 4.2: Schematic of the ψ representation

Now calculating the entanglement of (4.17) by concurrence, we find

$$\begin{aligned} \mathcal{C}(\psi') &= \mathcal{C}(\mathcal{U} \otimes \mathbb{1} \circ \mathcal{B} \otimes \mathbb{1}(\psi_{\Lambda\mathcal{V}})) \\ &= \mathcal{C}(\mathcal{B} \otimes \mathbb{1}(\psi_{\Lambda\mathcal{V}})), \end{aligned} \quad (4.18)$$

in the second line we neglected the unitary operation \mathcal{U} , since the entanglement is invariant under local unitary operations.

Using the result (4.9), which gives the concurrence evolution under filtering operation, the above equation takes the following form

$$\mathcal{C}(\psi') = \mathcal{C}(\psi)\mathcal{C}(\mathbb{1} \otimes \Lambda \mathcal{V}^*(\phi^+)), \quad (4.19)$$

where we have used that $\det B = \mathcal{C}(\psi)$. So the final and initial amount of

entanglement, $\mathcal{C}(\psi')$ and $\mathcal{C}(\psi)$, are connected by the term $\mathcal{C}(\mathbb{1} \otimes \Lambda \mathcal{V}^*(\phi^+))$. Nevertheless different of we wanted, the term $\mathcal{C}(\mathbb{1} \otimes \Lambda \mathcal{V}^*(\phi^+))$ depends from the initial state, since \mathcal{V}^* is the Schmidt operator related to the initial state ψ .

However, if we look the particular case with $D = 2$, then the initial 2×2 state in (4.11) is $|\psi_{2 \times 2}\rangle = \sum_{i,j} a_{ij} |i\rangle |j\rangle$ and transform as

$$\begin{aligned} \mathcal{C}(\mathbb{1} \otimes \Lambda(\psi_{2 \times 2})) &= \mathcal{C}(\psi_{2 \times 2}) \mathcal{C}(\mathbb{1} \otimes \Lambda \mathcal{V}^*(\phi^+)) \\ &= \mathcal{C}(\psi_{2 \times 2}) \mathcal{C}(\mathcal{V}^\dagger \otimes \Lambda(\phi^+)) \\ &= \mathcal{C}(\psi_{2 \times 2}) \mathcal{C}(\mathbb{1} \otimes \Lambda(\phi^+)). \end{aligned} \quad (4.20)$$

We use the fact that for 2×2 states $(\mathbb{1} \otimes A)|\phi_{2 \times 2}^+\rangle = (A^T \otimes \mathbb{1})|\psi_{2 \times 2}\rangle$, with A a 2×2 matrix and T denotes the transpose operation. Considering this particular case, we thus reach the relation obtained in [29], that is a factored form of the concurrence for 2×2 case. In the right side of (4.20) the first term relates to the initial state and the second one relates only to the evolution process. This equation tell us that any 2×2 pure state evolves qualitatively at the same way that a maximally entangled state evolve under the same arbitrary dynamical process.

4.1.3 A Statistical Approach of Entanglement Evolution in $2 \times D$ Systems

In order to find a factored relation for entanglement evolution in $2 \times D$ systems, here we will make use of an statistical approach. Instead of studying the entanglement behavior of a specific initial pure state which suffers the action of a dynamical channel over its D -dimensional subsystem, now we aim to study how the entanglement behaves when we take the average value of the concurrence over the set of uniformly distributed pure states. That is, we will derive from (4.19) a relation between the expectation value of the concurrence $\langle \mathcal{C}(\psi) \rangle$, related to this initial set of pure states $\{\psi\}$, and the expectation value of the concurrence $\langle \mathcal{C}(\psi') \rangle$ of the evolved set of states $\{\psi'\}$ (See Figure 4.3).

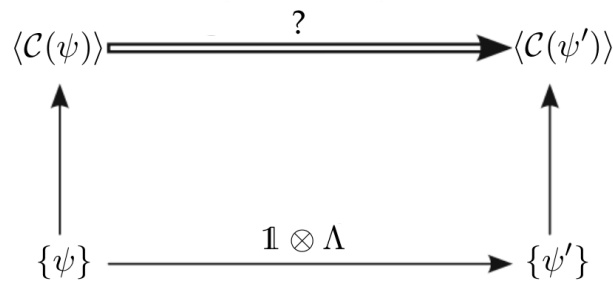


FIGURE 4.3: From a ensemble of uniformly distributed pure states which evolve under $\mathbb{1} \otimes \Lambda$, we want to find a entanglement dynamics relation between the expect value of the concurrence of the initial ensemble of states $\langle \mathcal{C}(\psi) \rangle$ and the expect value of the concurrence related to the final ensemble of states $\langle \mathcal{C}(\psi') \rangle$

Such an approach allows us to recognize some kind of typicality. The basic idea of typicality is: considering a set of states drawn according to

some specific distribution, there is "typicality" if there is some common feature (some observable for example) shared by this set of states, at a given time will yield very similar values [42]. Here we intend show that in high dimensions the vast majority of pure states share the same entanglement behavior when they undergo the same dynamical process, that is, there is typicality in entanglement dynamics for high dimensional cases.

We begin taking the expectation value of the derived relation (4.19)

$$\begin{aligned}\langle \mathcal{C}(\psi') \rangle &= \langle \mathcal{C}(\mathbb{1} \otimes \Lambda(\psi)) \rangle \\ &= \langle \mathcal{C}(\psi) \mathcal{C}(\mathbb{1} \otimes \Lambda \mathcal{V}^*(\phi^+)) \rangle\end{aligned}\quad (4.21)$$

where $\langle \cdot \rangle$ represent the expectation value. We assume that the set of pure states $\{\psi\}$ are picked randomly in a $2 \times D$ Hilbert space. So in the above equation we identify two dependent random variables in the right-hand side, the term $\mathcal{C}(\psi)$ and $\mathcal{C}(\mathbb{1} \otimes \Lambda \mathcal{V}^*(\phi^+))$, since ψ and V are connected.

So let us see how the right-hand side of (4.21) behaves when the space of D -dimensional part becomes large. First, consider two random variables X and Y , the covariance is given by:

$$\begin{aligned}\text{Cov}(X, Y) &= \langle XY \rangle - \langle X \rangle \langle Y \rangle \\ \Rightarrow \langle XY \rangle &= \langle X \rangle \langle Y \rangle + \text{Cov}(X, Y).\end{aligned}\quad (4.22)$$

Identifying $X = \mathcal{C}(\psi)$ and $Y = \mathcal{C}(\mathbb{1} \otimes \Lambda \mathcal{V}^*(\phi^+))$ in the above equation, we have:

$$\langle \mathcal{C}(\psi) \mathcal{C}(\mathbb{1} \otimes \Lambda \mathcal{V}^*(\phi^+)) \rangle = \langle \mathcal{C}(\psi) \rangle \langle \mathcal{C}(\mathbb{1} \otimes \Lambda \mathcal{V}^*(\phi^+)) \rangle + \text{Cov}[\mathcal{C}(\psi), \mathcal{C}(\mathbb{1} \otimes \Lambda \mathcal{V}^*(\phi^+))]. \quad (4.23)$$

So accordingly to the above equation, (4.21) becomes factored if $\text{Cov}[\mathcal{C}(\psi), \mathcal{C}(\mathbb{1} \otimes \Lambda \mathcal{V}^*(\phi^+))]$ goes to zero such that $\langle \mathcal{C}(\psi) \mathcal{C}(\mathbb{1} \otimes \Lambda \mathcal{V}^*(\phi^+)) \rangle \approx \langle \mathcal{C}(\psi) \rangle \langle \mathcal{C}(\mathbb{1} \otimes \Lambda \mathcal{V}^*(\phi^+)) \rangle$.

Let us see if this limit can be reached in large D -dimensional case using the covariance inequality (See Appendix):

$$\text{Cov}[\mathcal{C}(\psi), \mathcal{C}(\mathbb{1} \otimes \Lambda \mathcal{V}^*(\phi^+))] \leq \sigma[\mathcal{C}(\psi)] \sigma[\mathcal{C}(\mathbb{1} \otimes \Lambda \mathcal{V}^*(\phi^+))], \quad (4.24)$$

where σ is the standard deviation (defined by $\sigma(X) \equiv \text{Cov}(X, X)^{1/2}$). From [42], we know that the bigger D , the more concentrated is the entanglement distribution around its mean value. We confirm this result considering the distribution of the concurrence of an ensemble of pure states ψ . By cumulative density function and the expectation value of concurrence we note that, for high dimensions, the concurrence concentrates around $\mathcal{C}(\psi) = 1$ (See Figure 4.6). We also see that the standard deviation in high dimensions goes quickly to zero ($\sigma[\mathcal{C}(\psi)] \approx 0$), such that the right-hand side of (6.3) also goes to zero and the approximation $\text{Cov}[\mathcal{C}(\psi), \mathcal{C}(\mathbb{1} \otimes \Lambda \mathcal{V}^*(\phi^+))] \approx 0$ becomes valid.

Therefore for large D -dimensional case of $2 \times D$ systems, (4.21) becomes

$$\langle \mathcal{C}(\mathbb{1} \otimes \Lambda(\psi)) \rangle \approx \langle \mathcal{C}(\psi) \rangle \langle \mathcal{C}(\mathbb{1} \otimes \Lambda \mathcal{V}^*(\phi^+)) \rangle. \quad (4.25)$$

We can see that the Schmidt operators which compose set $\{V\}$ related to the $\{\psi\}$, exhibit an independent behavior in the high dimensional case. Therefore we find a relation of the entanglement in which for high dimensional

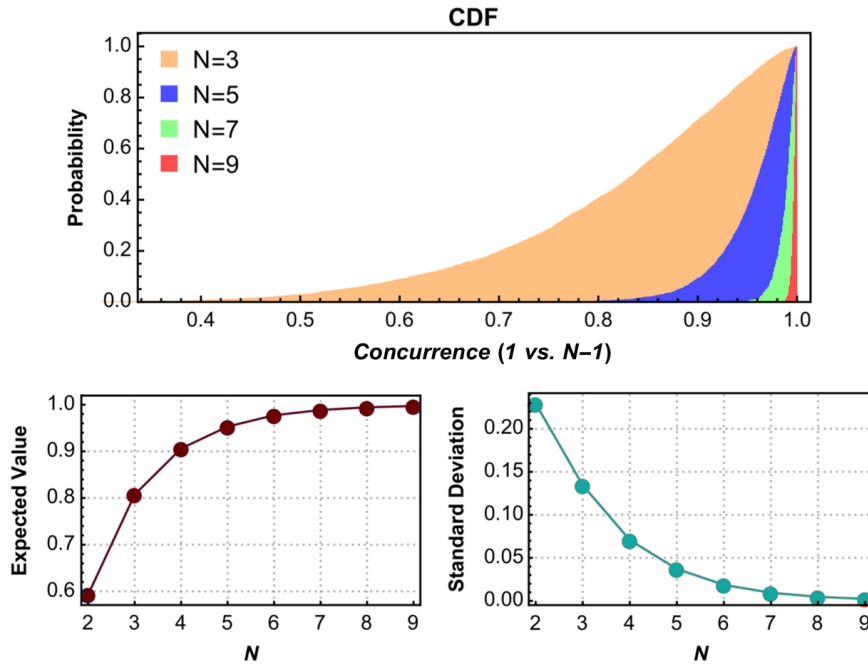


FIGURE 4.4: In the top the cumulative density function indicates that concurrence concentrates around $\mathcal{C}(\psi) = 1$. The evolution of the expected value of the concurrence and its standard deviation. In which we can see the values in which the concurrence concentrates and we note, from the standard deviation, that this fact occurs more intensely for higher dimensions.

systems the expectations values of concurrence $\langle \mathcal{C}(\psi) \rangle$ and $\langle \mathcal{C}(\mathbb{1} \otimes \Lambda(\psi)) \rangle$ are connected by the independent term $\langle \mathcal{C}((\mathbb{1} \otimes \Lambda \mathcal{V}^*(\phi^+)) \rangle$ that relates only to the channel Λ .

4.2 Entanglement in $2 \times D$ Coarse Grained Systems

Now we will illustrate the result (4.25) where the dynamical channel is a coarse graining channel Λ_{CG} .

In a realistic situation such coarse graining approach can describe a quantum measurement process in a laboratory scenario. Where in the action of measuring, a macroscopic detector (D -dimensional state ψ_D) interacts with a qubit (by an unitary transformation U). In the intrinsic interaction related to the measuring process, the detector and the qubit become entangled:

$$(\alpha|0\rangle + \beta|1\rangle) \otimes |\psi_D\rangle \xrightarrow{U} |\psi\rangle = \sum_{i=0}^1 \sum_{j=0}^{D-1} a_{ij} |i\rangle |j\rangle. \quad (4.26)$$

In a real situation we must keep in mind a crucial adversity, the experimentalist can not control all the degrees of freedom of the detector system, as it is composed by a huge number of particles. Instead, the handles only few effective degrees of freedom. So to properly describes the entanglement dynamics we must take into account the effective behavior of the detector.

So that this situation can be mapped by a coarse graining channel acting on the D -dimensional subsystem.

In this coupled system, a qubit is coupled to a qudit (D -dimensional system), and the qudit is described by an effective qubit due to the action of a coarse graining $\Lambda_{CG} : \mathcal{L}(\mathcal{H}_D) \rightarrow \mathcal{L}(\mathcal{H}_2)$ map:

$$\psi' = \mathbb{1} \otimes \Lambda_{CG}(\psi). \quad (4.27)$$

And the equation of expected value of concurrence (4.25) is rewritten as

$$\langle \mathcal{C}(\mathbb{1} \otimes \Lambda_{CG}(\psi)) \rangle = \langle \mathcal{C}(\psi) \rangle \langle \mathcal{C}((\mathbb{1} \otimes \Lambda_{CG}\mathcal{V}^*(\phi^+)) \rangle). \quad (4.28)$$

Let us look how the entanglement behaves in this coarse graining approach when we take different sizes of the D -dimensional part (different sizes of the detector). We use the coarse graining map developed in the last chapter (3.25) and its compositions (2.24). Then beyond dimension $D = 2$, we can construct coarse graining maps that act on subsystem of dimensions $D = 4$ and $D = 8$. In this way we are able to study the coarse-graining in follow situations:

$$\begin{aligned} \psi'_{2 \times 2} &= \mathbb{1} \otimes \Lambda_{CG}^{2 \rightarrow 1}(\psi_{2 \times 4}) \\ \psi'_{2 \times 2} &= \mathbb{1} \otimes \Lambda_{CG}^{4 \rightarrow 1}(\psi_{2 \times 16}) \\ \psi'_{2 \times 2} &= \mathbb{1} \otimes \Lambda_{CG}^{8 \rightarrow 1}(\psi_{2 \times 256}). \end{aligned} \quad (4.29)$$

Thus from an uniformly distributed set of pure states $\{\psi_{2 \times 4}\}$, $\{\psi_{2 \times 16}\}$ and $\{\psi_{2 \times 256}\}$, we can calculate $\langle \mathbb{1} \otimes \Lambda_{CG}^{2 \rightarrow 1}(\psi_{2 \times 4}) \rangle$, $\langle \mathbb{1} \otimes \Lambda_{CG}^{4 \rightarrow 1}(\psi_{2 \times 16}) \rangle$ and $\langle \mathbb{1} \otimes \Lambda_{CG}^{8 \rightarrow 1}(\psi_{2 \times 256}) \rangle$. In Figure 4.5 are shown the results. We observe that the concurrence almost vanishes as the dimension increases.

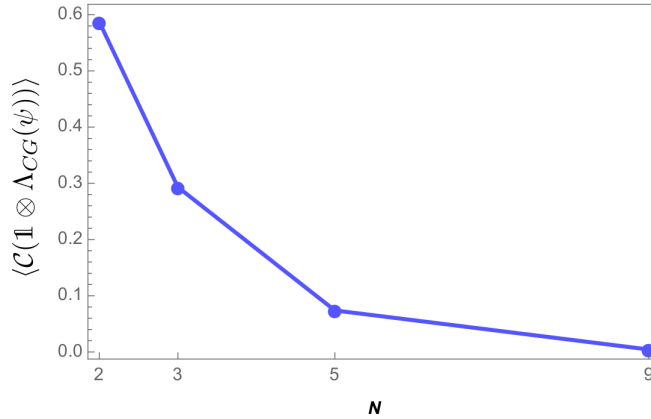


FIGURE 4.5: We observe that the entanglement decreases as the dimension of the detector increase. And in high dimensions ($D > 9$) the entanglement basically disappears.

Another interesting thing that we observe is that using the left side of (4.28), instead of using \mathcal{V} , using random unitary operators \mathcal{U}_R the distributions of $\mathcal{C}((\mathbb{1} \otimes \Lambda_{CG}\mathcal{V}^*(\phi^+))$ and $\mathcal{C}((\mathbb{1} \otimes \Lambda_{CG}\mathcal{U}_R(\phi^+))$ are very similar. Thus as consequence $\langle \mathcal{C}((\mathbb{1} \otimes \Lambda_{CG}\mathcal{V}^*(\phi^+)) \rangle$ and $\langle \mathcal{C}((\mathbb{1} \otimes \Lambda_{CG}\mathcal{U}_R(\phi^+)) \rangle$ and its standard deviation also are quite close, see Figure 4.6.

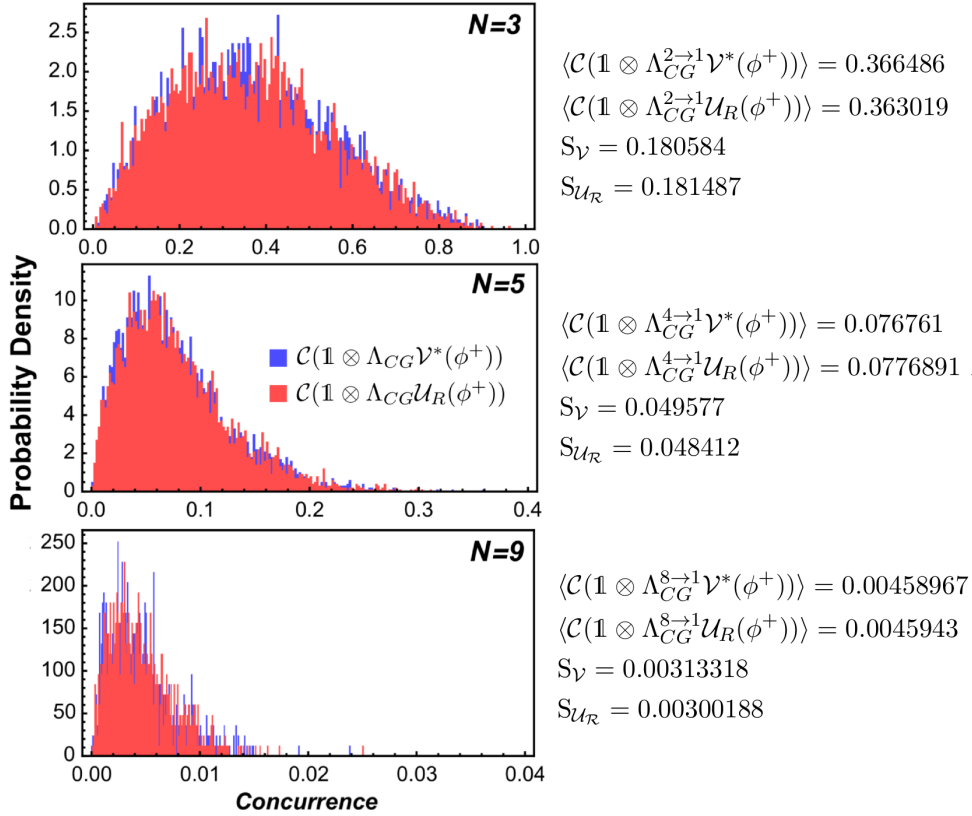


FIGURE 4.6: Here, are shown that the distributions of $\mathcal{C}(\mathbb{1} \otimes \Lambda_{CG} \mathcal{V}^*(\phi^+))$ and $\mathcal{C}(\mathbb{1} \otimes \Lambda_{CG} \mathcal{U}_R(\phi^+))$ are quite similar how much larger is the size of the system. $S_{\mathcal{V}}$ and $S_{\mathcal{U}_R}$ denotes the standard deviation respectively for $\mathcal{C}(\mathbb{1} \otimes \Lambda_{CG} \mathcal{V}^*(\phi^+))$ and $\mathcal{C}(\mathbb{1} \otimes \Lambda_{CG} \mathcal{U}_R(\phi^+))$. To construct this histogram, we sample over 3000 ($N = 3, N = 5$) or 1000 ($N = 9$) uniformly distributed pure initial states of N qubits and unitary operators \mathcal{U}_R .

So from this result, the equation (4.28) can be rewritten as

$$\langle \mathcal{C}(\mathbb{1} \otimes \Lambda_{CG}(\psi)) \rangle \approx \langle \mathcal{C}(\psi) \rangle \langle \mathcal{C}(\mathbb{1} \otimes \Lambda_{CG} \mathcal{U}_R(\phi^+)) \rangle. \quad (4.30)$$

In this case $\langle \mathcal{C}(\mathbb{1} \otimes \Lambda_{CG}(\psi)) \rangle$ are written into two independent terms. So the evolution of the set $\{\psi\}$ under a coarse graining process $\mathbb{1} \otimes \Lambda_{CG}$ can be mapped by the independent term $\langle \mathcal{C}(\mathbb{1} \otimes \Lambda_{CG} \mathcal{U}_R(\phi^+)) \rangle$. And more we can identify the combined action of the random unitary \mathcal{U}_R preceded by the coarse graining channel Λ_{CG} as a kind of random coarse graining that act on the qudit:

$$\langle \mathcal{C}(\mathbb{1} \otimes \Lambda_{CG}(\psi)) \rangle \approx \langle \mathcal{C}(\psi) \rangle \langle \mathcal{C}(\mathbb{1} \otimes \Lambda_{CG}^R(\phi^+)) \rangle, \quad (4.31)$$

where $\Lambda_{CG}^R \equiv \Lambda_{CG} \mathcal{U}_R$. So from this perspective we can conclude that the entanglement behavior observed in Figure 4.6, using the coarse graining map (3.25), can be extended to more general class of coarse graining channels Λ_{CG}^R .

Back to the measurement process where a detector interacts with a qubit. The above results shows that, as expected, that the larger is the detector, the

smaller is the amount of entanglement information that survives. That is, systems with many degrees of freedom, the coarse-grained entanglement quickly vanishes. Thus suggesting the decrease of the quantum features of the system, and consequently a classical description emerges.

Chapter 5

Conclusion and Perspectives

The present work aimed to study the entanglement dynamics behavior in coarse-grained systems. We started by developing a convenient coarse-graining description of the experimental realization [18]. In such experiment the researchers were able to detect entanglement in a spin chain realized with ultracold atoms in an optical lattice with single site detection. Since this accomplishment demands high-resolution microscopy, we developed a coarse-graining map that describes a simpler experimental entanglement detection, that in principle, would dispense this high experimental resources. Imagining a "blurred" detector that cannot resolve two sites in the lattice, we constructed a coarse graining map that describes such situation, taking the information of two spins degrees of freedom to a single one.

In the first part we developed such coarse-graining description of the realization [18]. Starting the spin dynamics with an initial impurity in the center of the chain, and using the coarse-graining map, we described how the entanglement behaves when it is taken different ranges of resolution of the chain. As expected, since the description of the spin entangled system is taken in a smaller dimensional space, it was verified a loss of entanglement information in the coarse-grained description. Both for concurrence and for negativity the amount of entanglement information decays when we consider the coarse-grained level of the spin-chain. Despite of this, a significant amount of entanglement still survives, such that we speculate that in a realistic experimental procedure the entanglement will still be detectable.

Therefore from our coarse-graining proposal, we can try to point out some future applications. From this work we hope to have contributed to the problem of description of the entangled systems. Taking the coarse-graining approach, in principle we can also model other physical situations. Here we constructed a map to describe a "blurred" detection of a spin-chain with a single impurity. However, the construction of a coarse-graining map is free to suit others physical situations. In an experimental scenario, realized with cold bosons in optical lattice, perhaps the immediate application would be to detect entanglement using the same lower bound proposed in [30], but now without the requirement of the single-spin detection accomplished in [18]. Through this experiment, we could verify how good our coarse-graining model is. Knowing details of the detector we can improve our coarse-graining map.

In the second part, in terms of concurrence, we derived an equation for entanglement dynamics in $2 \times D$ systems, where the D -dimensional part suffers the action of an arbitrary dynamical channel. We carried out this

task using the same method used in [43, 29, 44, 42]. Making use of a statistical approach, considering the average value of the concurrence for the set of uniformly distributed pure states, we deduced a factorized equation for quantum entanglement. We found an equation which only takes minimal information about the initial state (the set of uniformly distributed pure states) and the quantum channel related to the dynamical process. More specifically, we found that this set of initial states exhibit qualitatively the same entanglement dynamics that a maximally entangled pure state undergoes.

Next, as an application, we considered a $2 \times D$ system where the second subsystem undergoes the coarse-graining process developed in the first part of this work. Such situation can illustrate the measurement process, where a detector (D -dimensional system) interacts with a qubit (2-dimensional system). As expected, we saw that the larger the detector is, the smaller the amount of entanglement information survives. So, we conclude that maybe for few particle systems entanglement can be observed in a coarse-grained level. However for systems with many degrees of freedom, like a detector, the coarse-grained entanglement quickly vanishes, and a classical description emerges. This coarse-graining approach can shed light on the quantum-to-classical transition. As we saw, entanglement is hard to be observed since one would need a high control of the microscopic degrees of freedom of system (at least a huge part of it).

Chapter 6

Appendix

6.1 Probability Theory

For support, let us overview some basics results in probability theory. We will define some measures, like covariance and variance and will show an inequality that is equivalent to the Cauchy-Schwarz inequality.

6.1.1 Covariance and Variance

Considering X and Y as two random variables, the covariance is defined by [40]

$$\begin{aligned} \text{Cov}(X, Y) &\equiv \langle (X - \langle X \rangle)(Y - \langle Y \rangle) \rangle \\ &= \langle XY \rangle - \langle X \rangle \langle Y \rangle, \end{aligned} \quad (6.1)$$

where $\langle X \rangle$ is the expected value of X . In the second line, we use the linearity property of expectations.

The covariance relationship with inner product. Considering a, b constants, X, Y, Z random variables and $|f\rangle, |g\rangle, |h\rangle$ complex vectors, covariance and inner product share the following similar properties:

- Bilinear: $\text{Cov}(aX + bY, Z) = a\text{Cov}(X, Z) + b\text{Cov}(Y, Z)$ and $(a\langle f| + b\langle g|)|h\rangle = a\langle f|h\rangle + b\langle g|h\rangle$.
- Symmetric: $\text{Cov}(X, Y) = \text{Cov}(Y, X)$ and $\langle f|g\rangle = \langle g|f\rangle$.
- Positive semi-definite: $\text{Cov}(X, X) \geq 0$.

From the covariance between a random variable X with itself, another quantity can be defined:

$$\begin{aligned} \text{Var}(X) &\equiv \text{Cov}(XX) \\ &= \langle X^2 \rangle - \langle X \rangle^2, \end{aligned} \quad (6.2)$$

where $\text{Var}(X)$ is the variance of X .

6.1.2 Covariance Inequality

From the approach of covariance and variance, an important inequality can be derived

$$\text{Cov}(XY) \leq \sqrt{\text{Var}(X)\text{Var}(Y)}. \quad (6.3)$$

To prove this equation, let us define a random variable Z of the form:

$$Z = X - \frac{\text{Cov}(XY)}{\text{Var}(Y)}Y. \quad (6.4)$$

Calculating its variance

$$\begin{aligned} \text{Var}(Z) &= \text{Var}\left(X - \frac{\text{Cov}(XY)}{\text{Var}(Y)}Y\right) \\ &= \text{Var}(X) - \frac{\text{Cov}^2(XY)}{\text{Var}(Y)}, \end{aligned} \quad (6.5)$$

where we use the $\text{Var}(aX + bY) = a^2\text{Var}(X) + b^2\text{Var}(b)$. Since $\text{Var}(Z) \geq 0$ we have (6.5)

$$\text{Cov}(XY) \leq \sqrt{\text{Var}(X)\text{Var}(Y)}. \quad (6.6)$$

From the equivalence between covariance and inner product discussed before, the covariance inequality (6.6) can be related to the Cauchy-Schwarz inequality:

$$|\langle f|g \rangle|^2 \leq \langle f|f \rangle \langle g|g \rangle. \quad (6.7)$$

Bibliography

- [1] CS Adams and E Riis. "Laser cooling and trapping of neutral atoms". In: *Progress in quantum electronics* 21.1 (1997), pp. 1–79.
- [2] Luigi Amico et al. "Dynamics of entanglement in one-dimensional spin systems". In: *Physical Review A* 69.2 (2004), p. 022304.
- [3] Luigi Amico et al. "Entanglement in many-body systems". In: *Reviews of Modern Physics* 80.2 (2008), p. 517.
- [4] Leandro Aolita, Fernando de Melo, and Luiz Davidovich. "Open-system dynamics of entanglement: a key issues review". In: *Reports on Progress in Physics* 78.4 (2015), p. 042001.
- [5] Charles H Bennett and David P DiVincenzo. "Quantum information and computation". In: *Nature* 404.6775 (2000), pp. 247–255.
- [6] Charles H Bennett et al. "Teleporting an unknown quantum state via dual classical and Einstein-Podolsky-Rosen channels". In: *Physical review letters* 70.13 (1993), p. 1895.
- [7] Immanuel Bloch. "Quantum coherence and entanglement with ultracold atoms in optical lattices". In: *Nature* 453.7198 (2008), pp. 1016–1022.
- [8] Immanuel Bloch. "Quantum gases in optical lattices". In: *Physics World* 17.4 (2004), p. 25.
- [9] Immanuel Bloch. "Ultracold quantum gases in optical lattices". In: *Nature Physics* 1.1 (2005), pp. 23–30.
- [10] Andreas Buchleitner, Carlos Viviescas, and Markus Tiersch. *Entanglement and decoherence: foundations and modern trends*. Vol. 768. Springer Science & Business Media, 2008.
- [11] Man-Duen Choi. "Completely positive linear maps on complex matrices". In: *Linear algebra and its applications* 10.3 (1975), pp. 285–290.
- [12] C. Cohen-Tannoudji. *Quantum Mechanics*. Vol. 2. Wiley, 1991.
- [13] L-M Duan, E Demler, and Mikhail D Lukin. "Controlling spin exchange interactions of ultracold atoms in optical lattices". In: *Physical review letters* 91.9 (2003), p. 090402.
- [14] Jens Eisert, Marcus Cramer, and Martin B Plenio. "Colloquium: Area laws for the entanglement entropy". In: *Reviews of Modern Physics* 82.1 (2010), p. 277.
- [15] Matthew PA Fisher et al. "Boson localization and the superfluid-insulator transition". In: *Physical Review B* 40.1 (1989), p. 546.
- [16] Michael Foss-Feig. "Quantum simulation of many-body physics with neutral atoms, molecules, and ions". PhD thesis. Amherst College, 2013.

- [17] Takeshi Fukuhara et al. "Quantum dynamics of a mobile spin impurity". In: *Nature Physics* 9.4 (2013), pp. 235–241.
- [18] Takeshi Fukuhara et al. "Spatially resolved detection of a spin-entanglement wave in a Bose-Hubbard chain". In: *Physical review letters* 115.3 (2015), p. 035302.
- [19] JE Gentle. "Singular value factorization". In: *Numerical Linear Algebra for Applications in Statistics* (1998), pp. 102–103.
- [20] Markus Greiner et al. "Quantum phase transition from a superfluid to a Mott insulator in a gas of ultracold atoms". In: *nature* 415.6867 (2002), pp. 39–44.
- [21] Rudolf Grimm, Matthias Weidemüller, and Yurii B Ovchinnikov. "Optical dipole traps for neutral atoms". In: *Advances in atomic, molecular, and optical physics* 42 (2000), pp. 95–170.
- [22] Scott Hill and William K Wootters. "Entanglement of a pair of quantum bits". In: *Physical review letters* 78.26 (1997), p. 5022.
- [23] Michał Horodecki, Paweł Horodecki, and Ryszard Horodecki. "Separability of mixed states: necessary and sufficient conditions". In: *Physics Letters A* 223.1 (1996), pp. 1–8.
- [24] Ryszard Horodecki et al. "Quantum entanglement". In: *Reviews of modern physics* 81.2 (2009), p. 865.
- [25] J. D. Jackson. *Classical electrodynamics*. Wiley, 1962.
- [26] Richard Jozsa and Noah Linden. "On the role of entanglement in quantum-computational speed-up". In: *Proceedings of the Royal Society of London A: Mathematical, Physical and Engineering Sciences*. Vol. 459. 2036. The Royal Society. 2003, pp. 2011–2032.
- [27] Petar Jurcevic et al. "Quasiparticle engineering and entanglement propagation in a quantum many-body system". In: *Nature* 511.7508 (2014), pp. 202–205.
- [28] Norio Konno. "Limit theorem for continuous-time quantum walk on the line". In: *Physical Review E* 72.2 (2005), p. 026113.
- [29] Thomas Konrad et al. "Evolution equation for quantum entanglement". In: *Nature physics* 4.2 (2008), pp. 99–102.
- [30] Leonardo Mazza et al. "Detecting two-site spin-entanglement in many-body systems with local particle-number fluctuations". In: *New Journal of Physics* 17.1 (2015), p. 013015.
- [31] M. Nielsen and I. Chuang. *Quantum Computation and Quantum Communication*. Cambridge University Press, 2006.
- [32] Chad Orzel et al. "Squeezed states in a Bose-Einstein condensate". In: *Science* 291.5512 (2001), pp. 2386–2389.
- [33] Andreas Osterloh et al. "Scaling of entanglement close to a quantum phase transition". In: *Nature* 416.6881 (2002), pp. 608–610.
- [34] Belén Paredes et al. "Tonks–Girardeau gas of ultracold atoms in an optical lattice". In: *Nature* 429.6989 (2004), pp. 277–281.
- [35] Tim Rom et al. "State selective production of molecules in optical lattices". In: *Physical review letters* 93.7 (2004), p. 073002.

- [36] CF Roos et al. "Bell states of atoms with ultralong lifetimes and their tomographic state analysis". In: *Physical review letters* 92.22 (2004), p. 220402.
- [37] CF Roos et al. "Bell states of atoms with ultralong lifetimes and their tomographic state analysis". In: *Physical review letters* 92.22 (2004), p. 220402.
- [38] C Ryu et al. "Raman-induced oscillation between an atomic and a molecular quantum gas". In: *arXiv preprint cond-mat/0508201* (2005).
- [39] Jacob F Sherson et al. "Single-atom-resolved fluorescence imaging of an atomic Mott insulator". In: *Nature* 467.7311 (2010), pp. 68–72.
- [40] George W Snedecor and William G Cochran. *Statistical Methods*. Ames. 1967.
- [41] V Subrahmanyam. "Entanglement dynamics and quantum-state transport in spin chains". In: *Physical Review A* 69.3 (2004), p. 034304.
- [42] Markus Tiersch, Fernando De Melo, and Andreas Buchleitner. "Universality in open system entanglement dynamics". In: *Journal of Physics A: Mathematical and Theoretical* 46.8 (2013), p. 085301.
- [43] Markus Tiersch, Fernando de Melo, and Andreas Buchleitner. "Entanglement evolution in finite dimensions". In: *Physical review letters* 101.17 (2008), p. 170502.
- [44] Markus Tiersch et al. "Equation of motion for entanglement". In: *Quantum Information Processing* 8.6 (2009), pp. 523–534.
- [45] Guifré Vidal and Reinhard F Werner. "Computable measure of entanglement". In: *Physical Review A* 65.3 (2002), p. 032314.
- [46] Christof Weitenberg et al. "Single-spin addressing in an atomic Mott insulator". In: *Nature* 471.7338 (2011), pp. 319–324.
- [47] William K Wootters. "Entanglement of formation of an arbitrary state of two qubits". In: *Physical Review Letters* 80.10 (1998), p. 2245.
- [48] Ting Yu and JH Eberly. "Evolution from entanglement to decoherence of bipartite mixed" X" states". In: *arXiv preprint quant-ph/0503089* (2005).